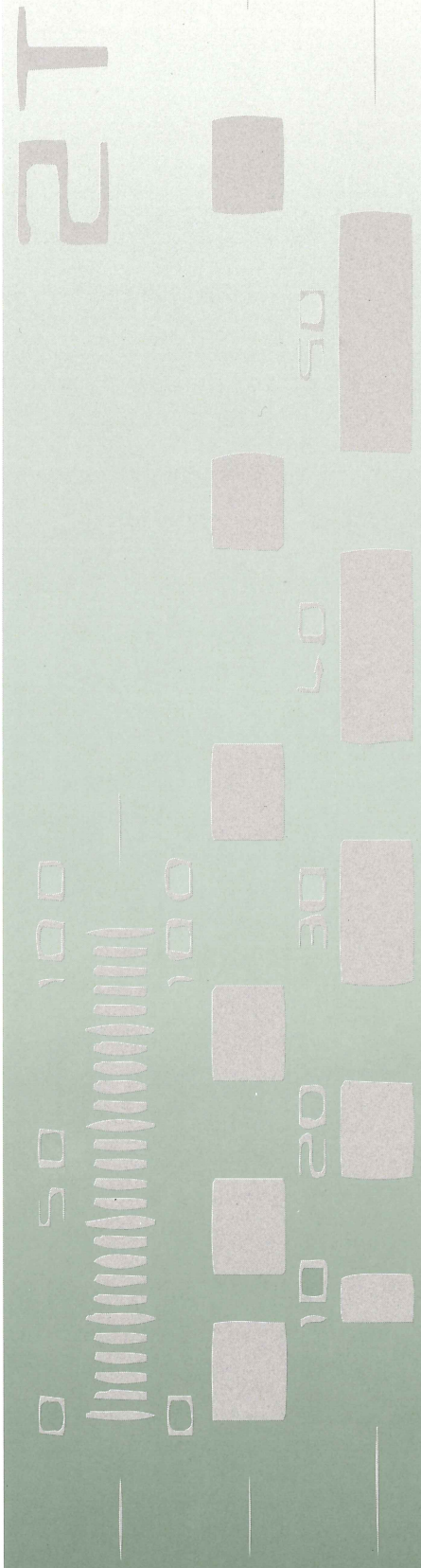
NPL Report COEM 34

REPORT

An Assessment of Four Techniques for Measuring the Effective Area of Optical Fibres

R Billington

October 1999



NPL
National Physical Laboratory

The National Physical Laboratory is operated on behalf of the DTI by NPL Management Limited, a wholly owned subsidiary of Serco Group plc

© Crown copyright 1999
Reproduced by permission of the Controller of HMSO

ISSN 1369 6807

National Physical Laboratory
Queens Road, Teddington, Middlesex, TW11 0LW

Extracts from this report may be reproduced provided the source is acknowledged

Approved on behalf of Managing Director, NPL
by D H Nettleton, Head of Centre for Optical and Environmental Metrology

Summary

Four techniques were assessed for use as the basis of a measurement service for the nonlinear effective area of single mode optical fibres. These were the far-field scan, near-field scan, variable aperture in the far-field and transverse offset techniques. In this report, the theory of each method and the relationships between them are discussed. Experimental data is presented for each method and issues relating to their accuracy are highlighted. It was found that all of the methods are highly sensitive to the numerical techniques used to analyse the results and that the dynamic range of measured data is a key factor.

Achieving sufficient dynamic range was found to be problematic with the near-field and transverse offset techniques due to insufficient fibre scan ranges. Both of these methods require precise alignment and linear translation of the test fibre on a micron scale, which was difficult to achieve and was prone to vibration sensitivity.

An important issue in effective area measurement is the handling of side-lobes found in the far-field angular intensity distribution. The measured intensity distribution can include distinct nulls where the amplitude of the electric field has changed sign. The measured intensity is given by the square of the field amplitude and therefore information on the sign of the amplitude is lost. Inverting odd numbered side-lobes in the electric field to give continuity before transforming to the near-field is found to increase the effective area of some fibres by up to 4% whilst having negligible effect on the mode-field diameter.

The variable aperture method is quick to perform but typically lacks the resolution and dynamic range to permit the side-lobes to be identified and inverted. An effective area measurement system based on the far-field scan technique offers the capability to calculate the effective area accurately by inverting side lobes. Measurements should then agree with those from a near-field scan-based system. Additionally, it also permits comparison with variable aperture measurement systems that do not invert side-lobes. The far-field scan technique therefore offers the most flexibility for intercomparison. Of the four techniques used, the far-field scan method was also found to have the highest repeatability

On the basis of these results, the far-field scan method has been selected as the foundation of the effective area measurement service to be developed under DTI contract MPU 8/52.2. Attention will now be concentrated on refining the numerical techniques used to calculate effective area from measured far-field intensity distributions.

Contents

1. Introduction 1

2. Definition of A_{eff} 2

2.1 Relationship of A_{eff} to MFD - "The Namihira Relation" 2

3. Fibres Used 6

4. The Direct Far-Field (DFF) Technique 7

4.1 Theory 7

4.2 Experimental Technique 9

4.3 Data Analysis 10

4.3.1 Results at 1549-nm Wavelength 13

4.3.2 Results at 1309.2-nm Wavelength 14

5. The Near-Field Scanning Technique 15

5.1 Data Analysis 17

5.1.1 Results at 1549-nm Wavelength 19

5.1.2 Results at 1309.2-nm Wavelength 20

5.2 The Effect of Offsets in Near-Field Intensity Data 20

6. The Variable Aperture in the Far-Field (VAFF) Technique 23

6.1 Theory 23

6.2 Experimental Technique 25

6.3 Data Analysis 26

6.3.1 Results at 1550-nm Wavelength 28

6.3.2 Results at 1310-nm Wavelength 28

6.4 Side-Lobe Inversion in Variable Aperture Data 28

7. The Transverse Offset Technique 32

7.1 Theory 32

7.2 Experimental Technique 33

7.3 Data Analysis 35

8. Summary of results 38

8.1 1549/1550-nm Results 38

8.2 1309.2/1310-nm Results 41

9. Conclusions 44

10. References 46

1. Introduction

Optical fibres in telecommunication systems now carry more channels and higher optical powers than ever before. Systems are operating in which the fibre carries such a high optical power density that signals can modify the transmission properties of the fibre. An optical channel can then affect how it and other channels propagate through the fibre - leading to *nonlinear effects*. By the term nonlinear, we mean that the optical signal leaving the fibre at a given wavelength does not change in proportion to changes in input power at that wavelength. Nonlinearity in fibres essentially appears as the conversion of power from one wavelength to another. Examples of nonlinearities include: self-phase modulation (SPM), cross-phase modulation (XPM), four-wave mixing (FWM), stimulated Raman scattering (SRS) and stimulated Brillouin scattering (SBS).

Nonlinear effects occur more efficiently in optical fibres than in bulk samples of their constituent materials because the optical field is confined to the small fibre core area for long distances. The confinement of the optical field within the core is achieved by the refractive index profile, which determines the field distribution of the fundamental mode. In general, optical power density is given by the optical power divided by the area over which it is distributed. The field of the fundamental mode of a single mode fibre bears little resemblance to the refractive index profile and therefore the area of the doped core region itself does not truly represent the area of the mode field. The *effective area*, A_{eff}, of the mode must be calculated from the field distribution but since this falls gradually to zero away from the fibre axis, some operational definition of effective area is required. A similar problem has been addressed before with respect to defining the mode field diameter (MFD) of single mode fibres. The MFD is used for calculating power losses due to fibre bending and offset splices and definitions have been derived based on the mode field distribution measured using a number of techniques [1]. The same techniques can be used to measure the mode field distribution of a single mode fibre and can therefore be used to calculate the effective area.

2. Definition of A_{eff}

All nonlinear effects are dependent upon the intensity of the electromagnetic field in the medium. However, it is the total optical power entering and leaving the fibre that is usually measured. Some method is required for converting between the two when comparing theoretical and experimental results. The measured optical power leaving a fibre is simply the integral of the intensity distribution over the entire fibre cross section. For a uniform intensity distribution, I, over a core of area A_{core}, the intensity could be calculated from the measured power, P_{meas}, using:

$$I = \frac{P_{meas}}{A_{core}} \qquad 2\text{-}1$$

However, the field in a single mode fibre is not evenly distributed or even fully contained within the core. It is larger at the fibre axis than near the core-cladding interface and extends into the cladding to a degree depending on the actual refractive index profile. Calculating a uniform intensity in the core using equation 2-1 will underestimate the value on the axis of the fibre and overestimate the value near the core-cladding interface.

The effective area parameter has been defined for the purposes of calculating nonlinear effects [2]. It is a single value, based on the modal field distribution, and can be used in equation 2-1 instead of A_{core} to calculate a value for the optical intensity. The effective area is defined as:

$$A_{eff} = \frac{2\pi\left(\int_0^\infty |E_a(r)|^2 r\,dr\right)^2}{\int_0^\infty |E_a(r)|^4 r\,dr} = \frac{2\pi\left(\int_0^\infty I(r) r\,dr\right)^2}{\int_0^\infty I^2(r) r\,dr} \qquad 2\text{-}2$$

where $E_a(r)$ is the amplitude and $I(r)$ is the intensity of the near-field of the fundamental mode at radius r from the axis of the fibre.

2.1 Relationship of A_{eff} to MFD - "The Namihira Relation"

In conventional step-index fibres, the mode-field is well-approximated by a Gaussian function of radius w at the $1/e$ amplitude points. In this case, the effective area can be shown simply to be:

$$A_{eff} = \pi w^2(\lambda) \qquad 2\text{-}3$$

where $2w(\lambda)$ is the Petermann-II mode-field diameter (MFD) of the fibre at wavelength λ. The mode-field diameter is defined in the near-field by [1]:

$$MFD_{NF} = 2\sqrt{2}\left\{\frac{\int_0^\infty |E_a(r)|^2 r\,dr}{\int_0^\infty [E_a'(r)]^2 r\,dr}\right\}^{1/2}, \qquad 2\text{-}4$$

and in the far-field by:

$$MFD_{FF} = 2\sqrt{2}\left\{\frac{\int_0^\infty |F(p)|^2 p\,dp}{\int_0^\infty |F(p)|^2 p^3\,dp}\right\}^{1/2}. \qquad 2\text{-}5$$

where $|F(p)|^2$ is the angular intensity distribution of the field radiated from the fibre endface and $p = k\sin(\theta)$. The wavenumber of the radiation, k, is given by the usual relation $k = 2\pi/\lambda$.

For fibres that do not share the simple step-index geometry of conventional single mode fibre, such as dispersion-shifted and dispersion-flattened fibres, the mode field cannot be approximated by a Gaussian function. The simple relationship between MFD and A_{eff} given by equation 2-3 no longer holds and alternative methods are required to calculate the effective area. An example of this is shown in Figure 1, in which theoretical Gaussian and non-Gaussian field distributions are shown that have the same MFD of 8.00-μm using equation 2-4. However, the effective area of the Gaussian distribution is calculated using equation 2-2 to be 50.3-μm^2 - in agreement with equation 2-3 - whereas that of the non-Gaussian is 52.8-μm^2. It can be seen from these results that apparently small variations in the mode field distribution can lead to a significant difference in nonlinear effective area.

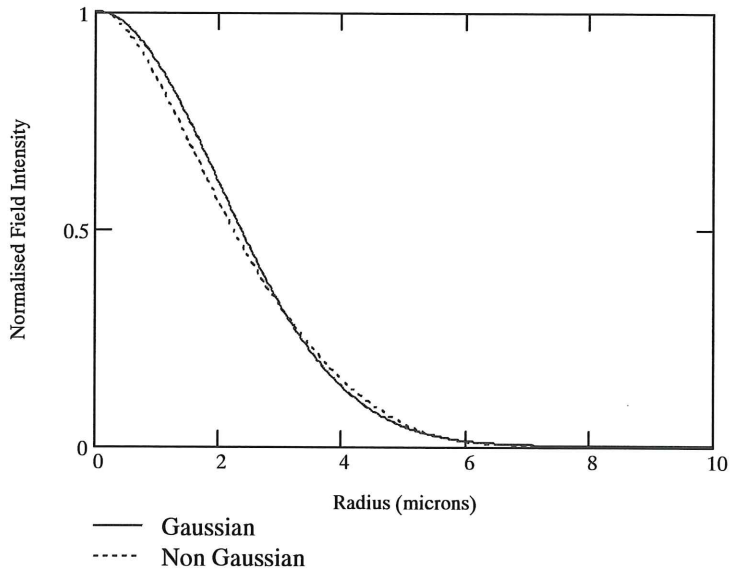


Figure 1. Gaussian and non-Gaussian near-field intensity distributions with the same Petermann-II MFD but different effective areas.

It has been proposed [3,4,5] that the effective area of various types of non-standard fibres can be calculated using equation 2-3 but including a correction factor, k_{Nam}, that depends on wavelength and the type of fibre. This has lead to the so-called "Namihira Relation":

$$A_{eff} = k_{Nam}\pi w^2(\lambda). \qquad 2\text{-}6$$

Published values from experimental data have suggested that the correction factor for dispersion-shifted fibres is approximately 0.95 and is only slightly dependent on the actual refractive index profile of the fibre. Similar measurements performed on large effective area fibres gave values of k_{Nam} in the range 1.03 to 1.17 and showed strong variations from one fibre to another [4]. The correction factor is dependent on wavelength and must be characterised as such for each fibre.

The advantage of the Namihira Relation is that mode-field diameter is a parameter that is routinely specified for all new fibres and which can be determined accurately by a number of well-established techniques. Most of these techniques do not actually involve calculating the mode-field distribution, $I(r)$, as relationships such as equation 2-5 have been derived that define the MFD in terms of other measured parameters. A large amount of test equipment is already installed in the marketplace that automatically measures MFD. Therefore, it would be useful to be able to calculate general correction factors to be applied to the MFD in order to calculate A_{eff} without the need to invest in new equipment to measure the mode-field distribution directly.

The disadvantage of using the correction factor k_{Nam} is its dependence on the fibre type. Initial investigations by Namihira using 12 different dispersion-shifted fibres (ITU-T G.653) at wavelengths between 1540-nm and 1574-nm showed that the average value of k_{Nam} to be 0.944 with a relatively small standard deviation of 0.002 [3]. The MFD and A_{eff} values in this case were calculated from the measured refractive-index profiles of the fibres. Later investigations used measured VAFF data to calculate these parameters [4,6]. The correction factor was determined experimentally by using the variable aperture technique to calculate the MFD $2w$ and the far-field intensity distribution $F(p)$. The far-field was then transformed to the near-field, $I(r)$, using the inverse Hankel transform. The near-field intensity distribution was then used to calculated the effective area, A_{eff}, which was then compared with πw^2. The correction factor for dispersion-shifted fibres was found to be relatively insensitive to the actual refractive index profile of the fibre. However, further investigations using fibres with large effective areas, non-zero dispersion shifted fibres (ITU-T G.655) and cut-off shifted fibres (ITU-T G.654) found k_{Nam} to be strongly dependent on the actual refractive index profile [4,5,6]. Therefore, the correction factor should be calculated for each type of G.655, G.654 or large effective area fibre. Hence, with the apparent exception of dispersion-shifted fibres, the same number of measurements are required to give the correction factor as are needed to find the effective area.

Another important point regarding values of k_{Nam} calculated from variable aperture data is the effect of side-lobes in the far-field radiation pattern, which are discussed in more detail in section 6.4. Our investigations illustrate that the VAFF technique can lead to a fibre-dependent underestimate of the effective area of the order of 2% that gives a similar underestimate in k_{Nam}.

3. Fibres Used

Six fibres were measured during this investigation. These were chosen to represent a broad range of fibre types. The fibres used were:

1. Corning Matched Cladding Fibre (serial no. 222313006411).

2. Corning LEAF-E Terrestrial Large Effective Area Fibre (serial no. 621758938807). Non-zero dispersion-shifted with positive dispersion at 1550-nm.

3. Corning SUBLEAF-E Submarine Large Effective Area Fibre (serial no. 321736069705).). Non-zero dispersion-shifted with negative dispersion at 1550-nm.

4. Sumitomo Dispersion-Shifted Fibre (serial no. 612007590).

5. Lucent True Wave Dispersion-Flattened Fibre (serial no. 991444960001).

6. Lucent All Wave Attenuation-Flattened Fibre (serial no. 004V19597D2CLD).

4. The Direct Far-Field (DFF) Technique

4.1 Theory

When the radiation propagating in a single mode fibre reaches a cleaved endface, it radiates from the fibre into the surrounding medium, which is usually air. The core of single mode fibres is typically 5 to 10-μm in diameter and is consequently comparable in size to the wavelength of the radiation - typically 1.3-μm to 1.65-μm. Under these circumstances, the light diffracts as it leaves the fibre and the resulting electromagnetic field evolves from a *near-field* distribution close to the fibre endface into a *far-field* distribution further away. The near-field being usually defined as the region within w^2/λ of the fibre endface and the far-field applies at distances greater than this.

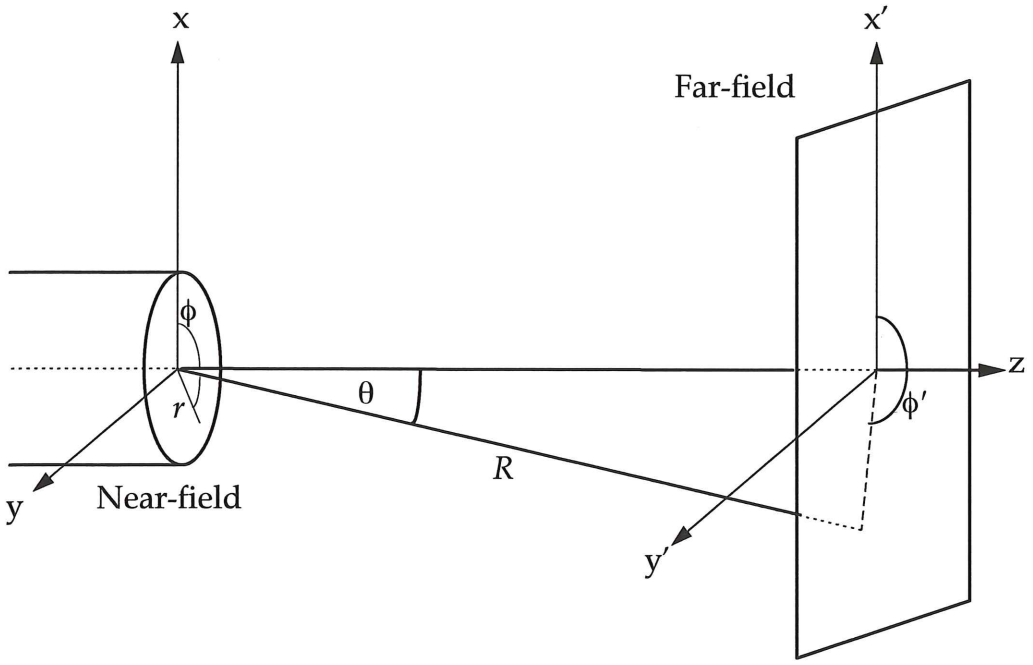


Figure 2. *Co-ordinates used to describe the near- and far-field radiation patterns of a single mode fibre.*

The amplitude of the radiation pattern in the far-field is related to that in the near-field by the diffraction integral [1,7]:

$$\psi(R,p) = O(\theta)\frac{k}{iR}\exp(ikR)\int_0^\infty E_a(r)J_0(rp)rdr \qquad 4\text{-}1$$

Co-ordinates R and θ are two of the spherical polar co-ordinates describing the point of observation as shown in Figure 2 and $J_0(rp)$ is the zeroth order Bessel function. The near- and far-field distributions are assumed to be independent of the rotational co-ordinate ϕ - an assumption that is valid only for cylindrically-symmetric fibres. $O(\theta)$ is an *obliquity factor* that should be

equal to $\cos(\theta)$ but is often assumed to be unity since the angles of observation for conventional single mode fibres are small [1]. However, fibres with smaller cores, such as dispersion-shifted fibres can generate far-field angular distributions in which the obliquity factor is more significant [7].

The observed far-field amplitude is given by the real part of the field distribution and therefore equation 4-1 can be re-written as:

$$F(p) = O(\theta)\int_0^\infty E_a(r)J_0(rp)rdr = O(\theta)\mathrm{HT}(E_a(r)) \qquad 4\text{-}2$$

Where $\mathrm{HT}(E_a(r))$ is the Hankel transform of the near-field distribution. The inverse Hankel transform is given by [7]:

$$E_a(r) = \int_0^\infty \left[\frac{F(p)}{O(\theta)}\right]J_0(rp)dp = \mathrm{HT}^{-1}\left[\frac{F(p)}{O(\theta)}\right] \qquad 4\text{-}3$$

Through equations 4-2 and 4-3, the near- and far-field radiation patterns can be related to each other. Although, as pointed out by Wittman and Young [7], the near field is not necessarily the same as the mode field since it applies in the free space just outside the fibre and not actually within the core. To reflect this, a distinction was drawn between the mode-field, $E_m(r)$ and the aperture field, $E_a(r)$. With the exception of the variable aperture data, Hankel transforms were performed numerically by approximating the function to be transformed by a series of uniform steps. The far-field points generated by the variable aperture method are fewer and more widely-spaced than those from the far-field scan method, so a slower quartic-fitting method was used in this case.

The standard TIA and ITU-T test methods for MFD ignore the difference between the aperture field and the mode field and also the obliquity factor is assumed to be unity [8,9]. This leads to the equation 2-5 for the MFD in terms of the far-field, which can also be expressed as:

$$MFD_{FF} = \frac{\sqrt{2}\lambda}{\pi}\left[\frac{\int_0^{\pi/2}|F(\theta)|^2\cos(\theta)\sin(\theta)d\theta}{\int_0^{\pi/2}|F(\theta)|^2\cos(\theta)\sin^3(\theta)d\theta}\right]^{1/2}. \qquad 4\text{-}4$$

Including the $\cos(\theta)$ obliquity factor, equation 4-4 becomes [7]:

$$MFD_{FF} = \frac{\sqrt{2}\lambda}{\pi}\left[\frac{\int_0^{\pi/2}|F(\theta)|^2 \tan(\theta) d\theta}{\int_0^{\pi/2}|F(\theta)|^2 \tan(\theta)\sin^2(\theta) d\theta}\right]^{1/2}. \qquad 4\text{-}5$$

4.2 Experimental Technique

The aim of the far-field scan technique is to accurately measure the angular distribution of the intensity of the field from the single mode fibre. The mode-field diameter, as used by ITU-T and the TIA is defined in terms of this intensity distribution and can be calculated directly from it as detailed in the previous section. However, for the purposes of calculating effective area, the far-field distribution must be converted into the near-field distribution for use in equation 2-2.

An experimental system for measuring the far-field radiation pattern from a single mode fibre is shown in Figure 3.

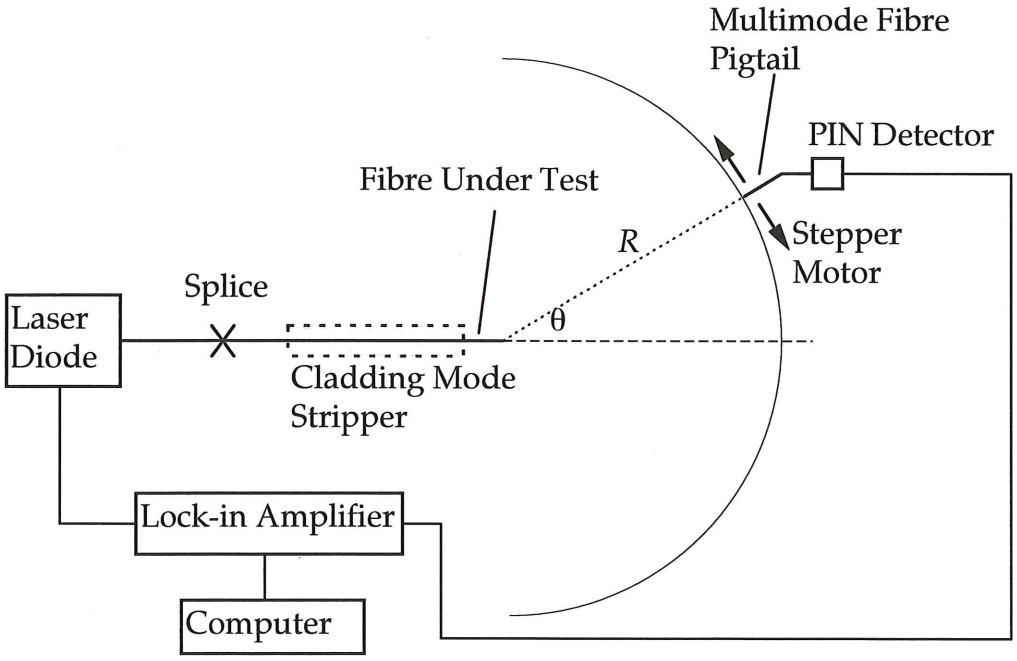


Figure 3. *Experimental system for measuring the far-field intensity distribution from a single mode optical fibre.*

The chopped output from a laser diode is launched into the fibre under test, which is then passed through a cladding mode stripper to remove any optical power not in the fundamental mode. The angular intensity distribution at radial distance $R \approx 20$-mm is then scanned using an InGaAs photodiode with a 100/140-μm multimode fibre pigtail. The detector fibre is mounted on a precision rotation stage that is stepped in fixed angular increments through a total arc of approximately 80°. The signal from the photodiode is amplified and passed to a current-to-voltage converter, giving a voltage proportional to

the optical power received by the fibre. The acceptance angle of the detector fibre is independent of the scan angle and therefore the received power is linearly proportional to the far-field intensity. The relative optical intensity as a function of angle is then recorded with the computer. An example of a far-field intensity distribution from a matched-cladding fibre at 1549-nm is shown in Figure 4.

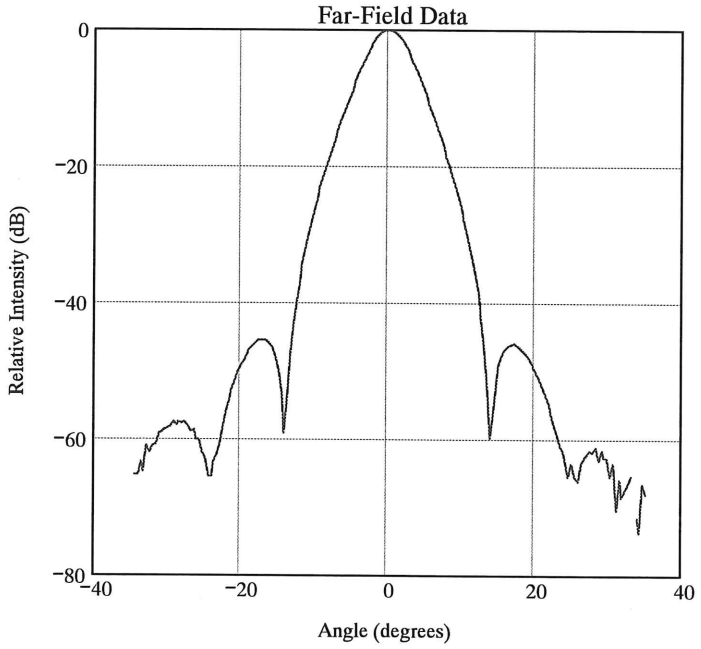


Figure 4. Example of a measured far-field intensity distribution, $|F(\theta)|^2$. Note that the intensity is plotted using a log scale and the magnitude of the first side-lobe is ~45-dB (optical) below the main peak.

4.3 Data Analysis

The mode field diameter can be calculated directly from the far-field intensity distribution, $|F(\theta)|^2$, using equation 4-4. The integration should theoretically be performed up to $\theta = \pi/2$. However, in practice, it is found that it typically converges within 40° although the actual value depends on the fibre type. To calculate effective area, $|F(\theta)|^2$ must be transformed into the near-field, $E_a(r)$, using equation 4-3. Once the near-field has been calculated, it can be used in equation 2-2 to calculate A_{eff}.

The numerical algorithms used to calculate the effective area from far-field data were tested using sample data given by the Telecommunications Industries Association (TIA) in their effective area test method recommendation document [10]. The far-field intensity distribution is shown in Figure 5.

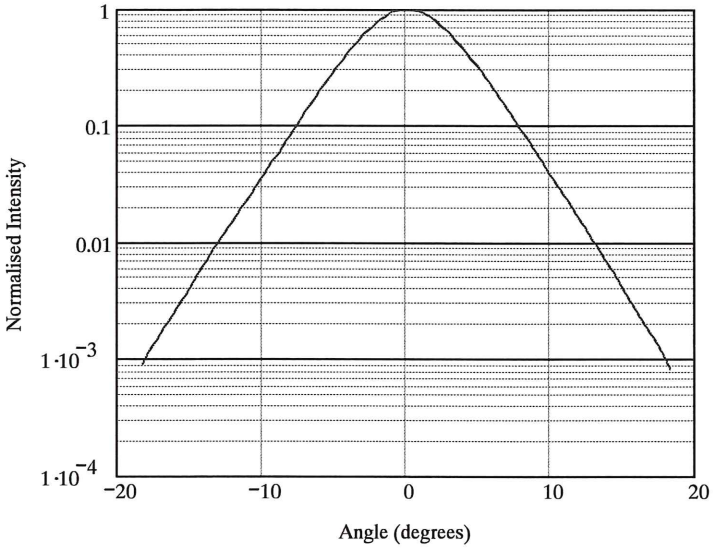


Figure 5. Far-field intensity distribution given in reference 10.

The far-field is given in reference 10 as two sets - one for each half of the scan. These were used to generate two symmetric sets of scan data so that an auto-centring routine could be tested that was used for experimental data. The far-field was used to calculate the mode-field diameter using equation 4-4 and was then transformed to the near-field, where equations 2-2 and 2-4 were used to calculate the effective area and mode-field diameter respectively. The near-field was generated for a set of 100 radial points in 0.15-μm steps from 0-μm to 15-μm. The MFD and effective area were evaluated using near-field points from 0-μm to the first point at which the intensity had fallen to below 0.01% of the peak value - corresponding to 40-dB of dynamic range - the minimum recommended by the TIA/EIA [10]. This restricted near-field was then transformed back to the far-field and equation 4-4 used to repeat the MFD calculation.

	LHS	RHS	Average
MFD from far-field (μm)	5.657	5.660	5.659
MFD from near-field (μm)	5.661	5.664	5.663
Aeff from near-field (μm)^2	24.198	24.236	24.217
MFD from regenerated far-field (μm)	5.653	5.656	5.655
TIA value for MFD (μm)	5.644	5.650	5.647
TIA value for Aeff (μm)^2			24.200

Table 1. Mode-field diameter and effective area values calculated from TIA far-field data. The effective area quoted for the TIA data is for the average of the two far-field half-scans.

The calculated and TIA values for the average MFD and effective area agree to within 0.3% and 0.1% respectively. The discrepancies are likely to be due to small differences in the numerical routines used to perform the Hankel transforms and calculate the MFDs and effective areas.

In analysing experimental far-field data for non-standard fibres, the calculation of the near-field from the far-field intensity is complicated by random noise and the presence of side-lobes in the far-field intensity distribution. Noise can lead to some negative intensity values that must be dealt with before the square root of the intensity distribution is taken to give the field amplitude. The side-lobes commonly found in far-field scans are recorded as positive intensity points but correspond to the square of negative amplitude values. In analysing the far-field data, the absolute values of the measured intensities were used to avoid producing imaginary amplitude values in the noise floor. After taking the square root of the intensities, the side-lobes were located manually and the amplitude of the odd-numbered lobes inverted. Figure 6 shows a far-field amplitude distribution of a sample of Lucent All Wave fibre at 1549-nm with the dashed lines indicating side-lobes that were inverted.

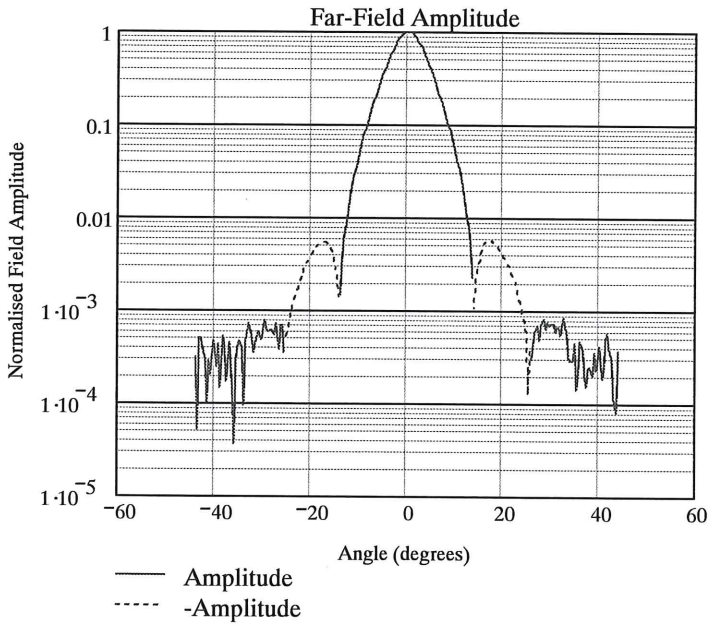


Figure 6. Far-field amplitude distribution calculated from a measured far-field intensity distribution. The dashed regions are side-lobes with negative amplitude that have been inverted to appear on the log plot.

The MFD and effective area values calculated from this data with and without inverting the sign of the side-lobe amplitudes are shown in Table 2.

Without Side-lobe Inversion	Left-Hand Side	Right-Hand Side	Average
MFD from far-field (μm)	10.244	10.261	10.253
MFD from near-field (μm)	10.244	10.260	10.252
Aeff from near-field (μm)^2	79.114	79.428	79.271
MFD from regenerated far-field (μm)	10.221	10.238	10.230
With Side-lobe Inversion			
MFD from far-field (μm)	10.244	10.261	10.253
MFD from near-field (μm)	10.243	10.259	10.251
Aeff from near-field (μm)^2	80.866	81.228	81.047
MFD from regenerated far-field (μm)	10.229	10.245	10.237

Table 2. Mode-field diameters and effective area calculated from far-field data for the Lucent All Wave fibre at 1549-nm.

Side-lobe inversion only affects those parameters calculated using the far-field amplitude rather than the intensity and therefore the far-field MFD values calculated using equation 4-4 are independent of side-lobe inversion. It can be seen that inverting the amplitude of the side-lobes increased the measured average effective area by approximately 2% in this case.

Far-field scans were measured for all six fibres listed in section 3 at two wavelengths - 1549.0-nm and 1309.2-nm. The MFD results include three values calculated from the far-field distribution. The first of these is the value supplied by the standard far-field MFD system at NPL on which the data was measured. The second far-field MFD is a value calculated from the raw data using the routine tested on the TIA sample data in Figure 5. The third value was calculated from the far-field distribution regenerated from the near-field used to calculate A_{eff}.

Results are presented with and without the far-field side lobes inverted. Fibre types marked with an asterisk did not exhibit any side-lobes. The Namihira factor was calculated for each fibre using equation 2-6 and taking the mode-field radius from the MFD given by the far-field system.

4.3.1 Results at 1549-nm Wavelength

The MFD and effective area values calculated from the far-field data are shown below. The standard deviations on the Namihira factors were calculated using:

$$\sigma_{kNam} = kNam\sqrt{\left(\frac{4}{\pi MFD^2}\right)^2 \sigma_{Aeff}^2 + \left(\frac{-8}{\pi MFD^3}\right)^2 \sigma_{MFD}^2} \qquad 4\text{-}6$$

Where σ_{Aeff} and σ_{MFD} represent the standard deviations on the effective area and mode-field diameter respectively. This gives a worst-case value for σ_{kNam} by assuming that that MFD and effective area are uncorrelated. Preliminary investigations have indicated that there is correlation and that σ_{kNam} may be reduced by up to a factor of 3, depending on the fibre type.

With Side-lobe Inversion	MFD From Far-Field System (μm)	Standard Deviation (μm)	Far-Field MFD (μm)	Standard Deviation (μm)	Near-Field MFD (μm)	Standard Deviation (μm)	Effective Area (μm)^2	Standard Deviation (μm)^2	Namihira Factor, k	Standard Deviation
Attenuation Flattened	10.250	0.006	10.249	0.015	10.247	0.015	80.936	0.227	0.981	0.003
Dispersion Flattened	8.395	0.011	8.394	0.016	8.393	0.015	53.835	0.197	0.973	0.004
Matched Cladding	10.424	0.014	10.423	0.019	10.421	0.019	83.391	0.305	0.977	0.004
Dispersion Shifted*	7.924	0.004	7.923	0.008	7.923	0.008	46.050	0.089	0.934	0.002
LEAF -'ve Dispersion*	9.100	0.017	9.099	0.023	9.099	0.023	67.250	0.295	1.034	0.006
LEAF +'ve Dispersion*	9.441	0.012	9.440	0.052	9.439	0.052	68.399	0.580	0.977	0.008
Without Side-lobe Inversion										
Attenuation Flattened	10.250	0.006	10.249	0.015	10.248	0.015	79.195	0.242	0.960	0.003
Dispersion Flattened	8.395	0.011	8.394	0.016	8.394	0.016	52.403	0.191	0.947	0.004
Matched Cladding	10.424	0.014	10.423	0.019	10.423	0.019	81.656	0.307	0.957	0.004
Dispersion Shifted*	7.924	0.004	7.923	0.008	7.923	0.008	46.050	0.089	0.934	0.002
LEAF -'ve Dispersion*	9.100	0.017	9.099	0.023	9.099	0.023	67.250	0.295	1.034	0.006
LEAF +'ve Dispersion*	9.441	0.012	9.440	0.052	9.438	0.052	68.399	0.580	0.977	0.008

Table 3. Mode-field diameters and effective areas at 1549-nm calculated from far-field scan data.

4.3.2 Results at 1309.2-nm Wavelength

The same parameters were calculated from the far-field scan data at 1309.2-nm and are shown below. Side lobes were identified in the far-fields of all fibres except for the large effective area fibre with positive dispersion in the 1550-nm region.

With Side-lobe Inversion	MFD From Far-Field System (μm)	Standard Deviation (μm)	Far-Field MFD (μm)	Standard Deviation (μm)	Near-Field MFD (μm)	Standard Deviation (μm)	Effective Area (μm)^2	Standard Deviation (μm)^2	Namihira Factor, k	Standard Deviation
Attenuation Flattened	9.140	0.003	9.138	0.009	9.138	0.009	66.385	0.132	1.012	0.002
Dispersion Flattened	7.016	0.012	7.015	0.015	7.015	0.015	38.467	0.141	0.995	0.005
Matched Cladding	9.257	0.016	9.256	0.018	9.255	0.018	67.786	0.267	1.007	0.005
Dispersion Shifted	6.364	0.016	6.363	0.017	6.364	0.017	29.747	0.157	0.935	0.006
LEAF -'ve Dispersion	6.677	0.045	6.677	0.053	6.678	0.053	34.107	0.538	0.974	0.020
LEAF +'ve Dispersion*	7.179	0.009	7.178	0.027	7.178	0.027	38.841	0.260	0.960	0.007
Without Side-lobe Inversion										
Attenuation Flattened	9.140	0.003	9.138	0.009	9.142	0.009	64.126	0.132	0.977	0.002
Dispersion Flattened	7.016	0.012	7.015	0.015	7.015	0.015	36.967	0.141	0.956	0.005
Matched Cladding	9.257	0.016	9.256	0.018	9.259	0.018	65.626	0.258	0.975	0.005
Dispersion Shifted	6.364	0.016	6.363	0.017	6.363	0.017	29.664	0.156	0.933	0.006
LEAF -'ve Dispersion	6.677	0.045	6.677	0.053	6.677	0.053	34.044	0.540	0.972	0.020
LEAF +'ve Dispersion*	7.179	0.009	7.178	0.027	7.178	0.027	38.841	0.260	0.960	0.007

Table 4. Mode-field diameters and effective areas at 1309.2-nm calculated from far-field scan data.

5. The Near-Field Scanning Technique

The advantage of scanning the near-field intensity distribution of the test fibre directly is that there is no need for mathematical transformations of the measured data. If the intensity distribution of the aperture field, $|E_a(r)|^2$, is measured then it can be input directly into equation 2-2 to give the effective area. The main difficulty with measuring the near-field is that it extends over very small area - typically 5-10-μm in diameter. Consequently, optics are required to produce a magnified image of the field that can be scanned radially using a detector with a pinhole in front or a fibre pigtail. The optical system must be carefully constructed to ensure that the magnified image is a faithful representation of the end of the test fibre. A high numerical aperture system is required to avoid blurring the image by truncating the angular distribution of the field leaving the fibre. This becomes more of a problem for fibres with particularly small cores since the field diverges more quickly outside the fibre.

The near-field scanning system used at NPL is shown schematically in Figure 7. The current from the photodiode detector is proportional to the optical power accepted by the pinhole or detecting fibre. This is linearly converted to a voltage, which is then also proportional to the power and therefore to the near-field intensity. It is the voltage signal as a function of the radius of the near-field sample point that constitutes the measured data. Scanning is performed by moving the test fibre with stepper motors and using interferometers to measure the position of the fibre. The advantage of this method over moving the detector is that the magnification of the imaging system does not need to be determined. The fibre position is stepped in nominally uniform increments of 0.1-μm with standard deviation of typically 0.004-μm.

Initial fibre positioning is performed using a confocal system in which the beamsplitter after the objective lens creates two identical optical paths. The pinhole detector and the endface of the confocal single mode fibre are the same distance from the focal point of the objective lens. The test fibre can be positioned precisely at the focal point of the objective lens by switching the laser source to emerge from the confocal fibre. By measuring and maximising the optical power launched backwards into the test fibre, it can be optimally positioned.

An example of a measured near-field from a standard matched-cladding fibre is shown in Figure 8.

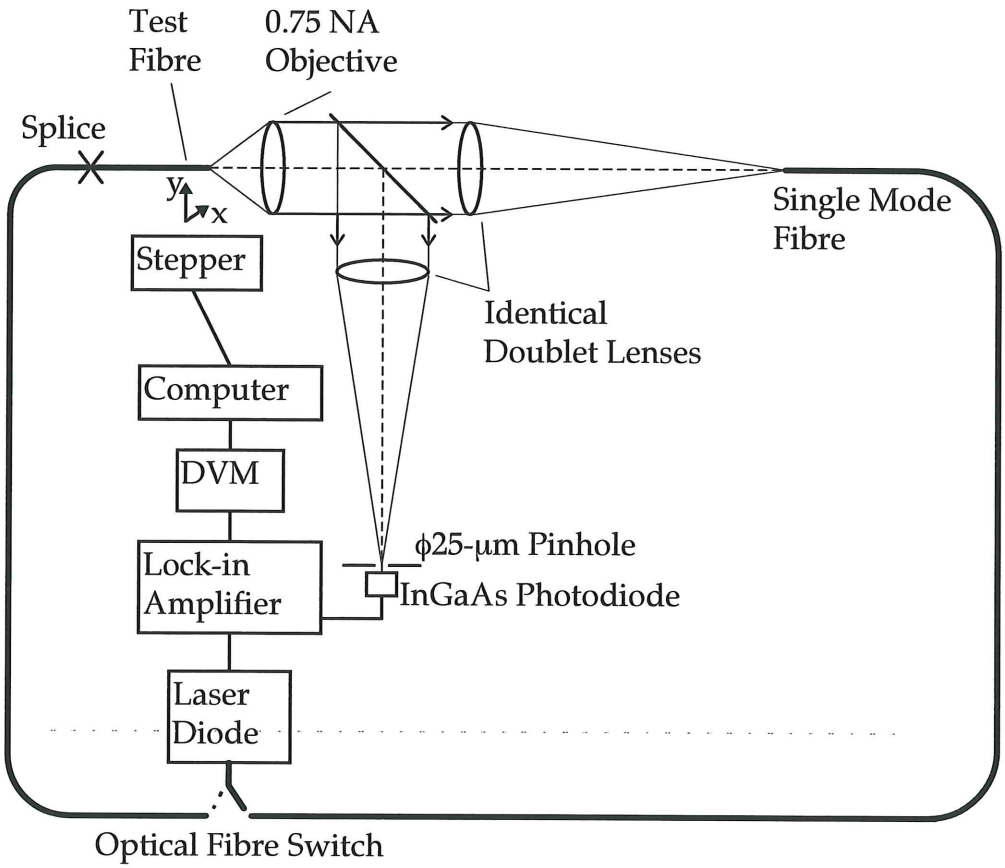


Figure 7. *Confocal near-field scanning system used at NPL to measure the near-field of a single mode fibre.*

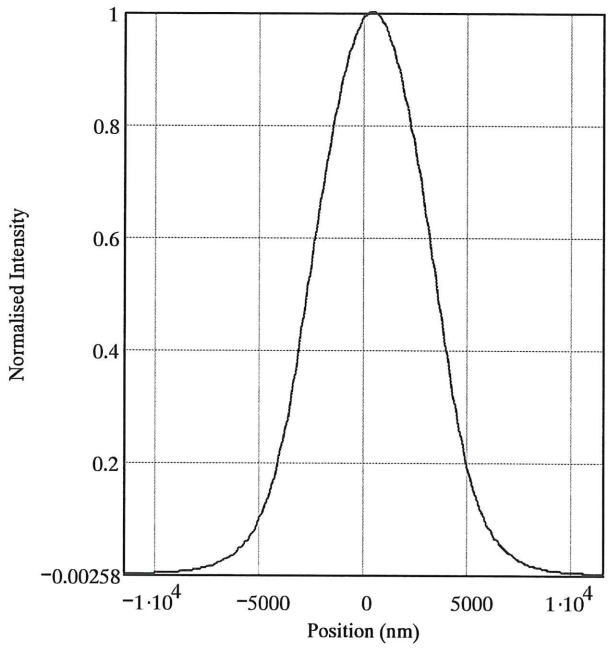


Figure 8. *Example of a measured near-field intensity distribution from a matched-cladding fibre.*

5.1 Data Analysis

The near-field scanning technique measures the relative intensity of the aperture field as a function of radius, $I(r) = |E_a(r)|^2$ as a set of voltages. These are usually normalised to 1 at the centre of the near-field distribution so that the data set consists of values of $I(r)/I(0)$. The TIA/EIA standard document for effective area measurement contains an example of such a data set for checking effective area calculations [10]. This was used to verify the numerical routines used to evaluate equation 2-2. The single-sided sample data set was used to form a symmetrical double-sided intensity distribution of the same form as the experimental data so that the automatic centring routine could be tested. The accompanying far-field data in reference 10 matches that in the TIA/EIA mode-field diameter document FOTP-164 [8] and so the MFD value for the near-field data in ref. 10 was taken from this document.

	Left-Hand Side	Right-Hand Side	Average
MFD from near-field (μm)	5.654	5.654	5.654
Aeff from near-field (μm)^2	24.162	24.162	24.162
MFD from regenerated far-field (μm)	5.645	5.645	5.645
TIA value for MFD (μm)			5.647
TIA value for Aeff (μm)^2			24.200

Table 5. Mode-field diameter and effective area values calculated from TIA/EIA sample data.

From these results, it can be seen that the near-field MFD values agree to within 0.1% and the effective areas to within 0.2%.

The experimental data measured at NPL included a small voltage offset introduced by a fault in the lock-in amplifier. The offset was estimated for the sets of scans performed on each fibre based on dark readings and the offset required to give exponentially decaying near-field intensities far into the cladding. An example of this process is shown in Figure 9. The effect of bias voltages on the calculated MFD and effective area is assessed in section 5.2.

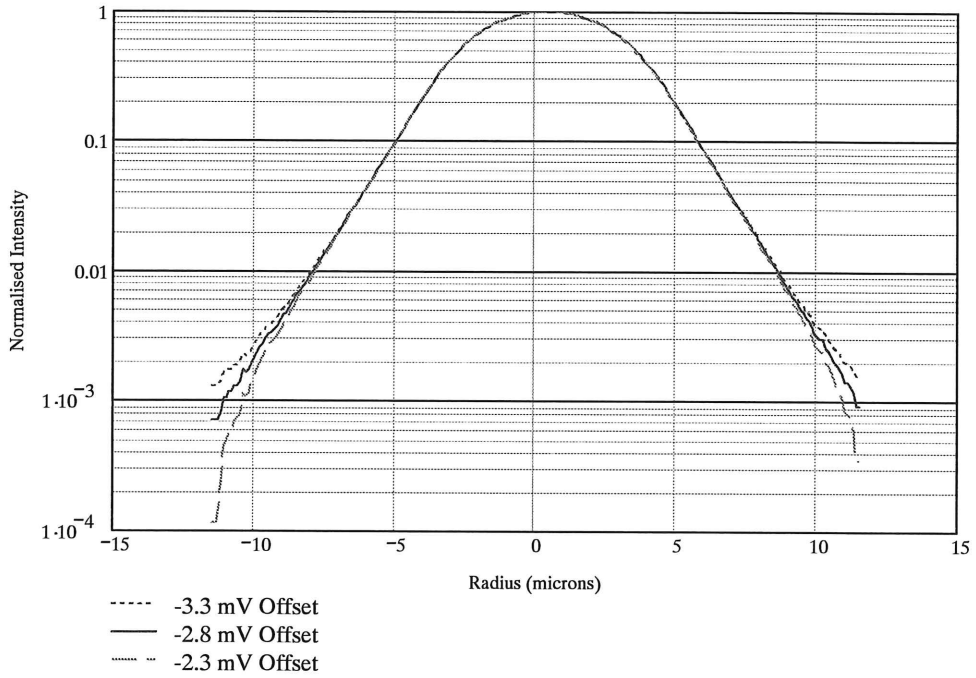


Figure 9. Measured near-field intensity distribution leaving the attenuation-flattened fibre. The bias in the measured voltages was estimated to be -2.8-mV based on the linearity of the tails of the near-field on a log scale.

After the bias correction had been made, the near-field intensity distribution was split into two halves by fitting a Gaussian function to the data points with greater than 0.5 normalised intensity. The Gaussian curve was used to estimate the position and intensity of the peak. A point was then inserted into the left and right-hand side data sets to represent the intensity at zero radius and the data was normalised to this value. Finally, equally-spaced data points were interpolated from the measured data and then inserted on-axis point using a sliding quadratic fitting function. The left and right-hand near-field data sets derived from the near-field with -2.8-mV bias in Figure 9 are shown in Figure 10 together with a near-field intensity distribution calculated from a far-field scan of the same fibre at the same wavelength.

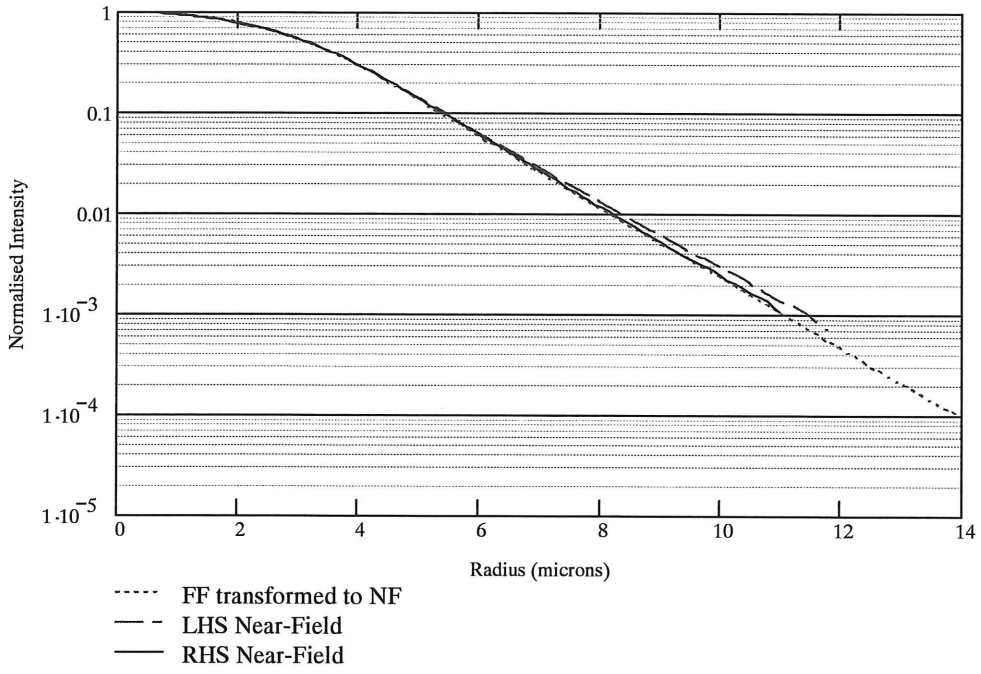


Figure 10. *Comparison of the two halves of the measured near-field in Figure 9 assuming -2.8-mV bias with the near-field derived from a far-field scan of the same fibre.*

The dynamic range of the near-field data was typically between 30-dB and 40-dB. Few results had the 40-dB dynamic range required for the evaluation of the MFD and effective area integrals out to the 0.01% normalised intensity points. Therefore, 30-dB was chosen as the cutoff point for these calculations. The results are compared with MFD and effective area values calculated from the far-field measurements with side lobes inverted. However, whereas the results presented in section 4.3 used 40-dB dynamic range of the near-field distribution, the results presented here were calculated using only 30-dB for comparison with the near-field measurements.

5.1.1 Results at 1549-nm Wavelength

Measurements were performed on five of the six test fibres using the same source as for the far-field measurements. A poor signal-to-noise ratio prevented measurements on the dispersion-flattened fibre at this wavelength. The Namihira conversion factors were calculated from the MFD and effective areas derived from the near-field data.

Results at 1549-nm	MFD From Far-Field System (μm)	Standard Deviation (μm)	Transformed FF- to NF MFD at 30-dB	Standard Deviation (μm)	Measured Near-Field MFD (μm)	Standard Deviation (μm)	Effective Area from Far-Field (μm)^2 using 30-dB	Standard Deviation (μm)^2	Effective Area from Near-Field using 30-dB (μm)^2	Standard Deviation (μm)^2	Namihira Factor, k	Standard Deviation
Attenuation Flattened	10.250	0.006	10.261	0.015	10.384	0.075	80.630	0.226	82.377	0.906	0.973	0.017
Dispersion Flattened	8.395	0.011	-	-	-	-	-	-	-	-	-	-
Matched Cladding	10.424	0.014	10.434	0.019	10.483	0.038	83.042	0.307	83.947	0.563	0.973	0.009
Dispersion Shifted	7.924	0.004	7.930	0.008	7.997	0.076	45.715	0.089	46.597	0.877	0.928	0.023
LEAF -'ve Dispersion	9.100	0.017	9.111	0.023	9.218	0.081	66.733	0.305	68.450	1.469	1.026	0.029
LEAF +'ve Dispersion	9.441	0.012	9.451	0.052	9.607	0.130	67.888	0.574	70.147	2.019	0.968	0.037

Table 6. Mode-field diameters and effective areas at 1549-nm calculated from near-field scan data.

5.1.2 Results at 1309.2-nm Wavelength

Results at 1309.2-nm	MFD From Far-Field System (μm)	Standard Deviation (μm)	Transformed FF to NF MFD (30-dB)	Standard Deviation (μm)	Near-Field MFD (μm)	Standard Deviation (μm)	Effective Area from Far-Field using 30-dB (μm)^2	Standard Deviation (μm)^2	Effective Area from Near-Field using 30-dB (μm)^2	Standard Deviation (μm)^2	Namihira Factor, k	Standard Deviation
Attenuation Flattened	9.140	0.003	9.151	0.009	9.223	0.075	66.182	0.131	67.049	0.777	1.004	0.020
Dispersion Flattened	7.016	0.012	7.017	0.015	7.078	0.043	38.257	0.147	38.842	0.380	0.987	0.015
Matched Cladding	9.257	0.016	9.268	0.018	9.385	0.112	67.569	0.267	69.010	1.329	0.998	0.031
Dispersion Shifted	6.364	0.016	6.370	0.016	6.415	0.048	29.562	0.164	30.011	0.429	0.929	0.018
LEAF -'ve Dispersion	6.678	0.045	6.688	0.053	6.744	0.060	33.875	0.530	34.442	0.678	0.964	0.025
LEAF +'ve Dispersion	7.179	0.009	7.188	0.028	7.266	0.085	38.567	0.258	39.381	0.946	0.950	0.030

Table 7. Mode-field diameters and effective areas at 1309.2-nm calculated from near-field scan data.

5.2 The Effect of Offsets in Near-Field Intensity Data

As stated previously, the near-field intensity data included a bias voltage from the lock-in amplifier. The value of this offset was estimated for each data set by examining near-field data on a logarithmic voltage scale. Far into the uniform cladding of an optical fibre, the amplitude of the fundamental fibre mode decays approximately exponentially. Bias voltages were estimated based on the values that produced exponentially-decaying tails in the measured near-field intensity distributions. The assumption of exponentially-decaying near-field intensity distributions is supported by near-fields calculated from measured far-field data via the Hankel transform. Examples of these are shown in Figure 11 for two different fibre types.

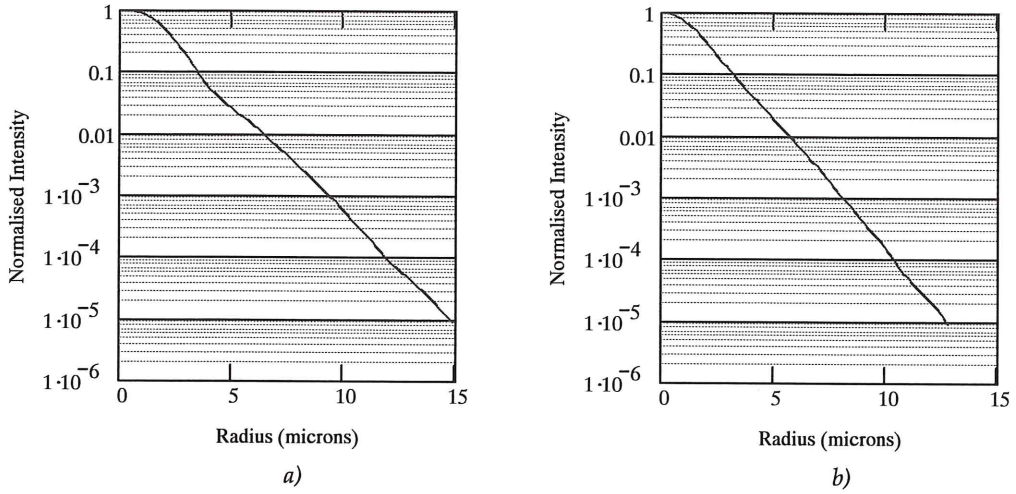
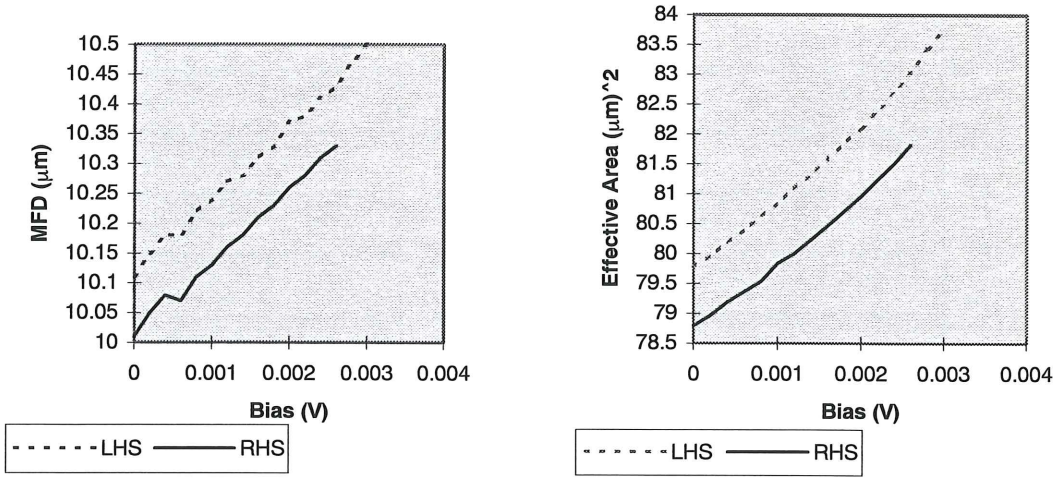


Figure 11. *Near-field intensity distributions calculated from measured far-field distributions at 1549-nm for a) the dispersion-flattened and b) the dispersion-shifted fibre.*

The MFDs and effective areas were calculated using a fixed dynamic range of near-field data. With a negative bias on the data, the dynamic range is infinite because the minimum intensity is negative. However, correcting the data for the bias shifted the minimum intensity above zero and limited the dynamic range. For our experimental data, the maximum dynamic range of the bias-corrected intensity was typically 30-40-dB and 30-dB was used as the cut-off point for the evaluation of MDF and A_{eff}. From calculations of MFD and A_{eff} based on near-fields derived from far-field data with side-lobes inverted, the effect of a 30-dB cut-off rather than 40-dB can be assessed. Comparing column 5 of Table 4 and column 3 of Table 6, the use of 30-dB rather than 40-dB dynamic range in the near-field is predicted to increase the MFD by approximately 0.1% at 1549-nm. Conversely, the effective area is predicted to decrease by up to 1%. These are the systematic errors to be expected due to using 30-dB dynamic range of near-field data rather than 40-dB.

For a fixed dynamic range of 30-dB the effect of varying the bias voltage for a near-field scan on the attenuation-flattened fibre is illustrated below. The offset due to the lock-in amplifier was negative for all scans and therefore the bias voltages applied were all positive. It can be seen that increasing the bias voltage increases both the MFD and the effective area and that the values do not converge before the offset reduces the dynamic range to less than 30-dB.



a) *b)*

Figure 12. a) MFD and b) A_{eff} calculated from the two halves of a measured near-field scan as a function of the voltage offset applied to the data. The curves stop at the points where the dynamic range falls below 30-dB.

Clearly, offsets such as this can significantly affect the calculated values of MFD and effective area. For this particular scan, the variations in MFD and A_{eff} are approximately 0.13-μm/mV and 1.5-μm^2/mV (to first order). For an uncertainty of ±0.5-mV on the bias voltage, this gives MFD and A_{eff} uncertainties of ±0.07-μm and ±0.8-μm^2 respectively, which represent approximately 1-1.5% uncertainties for this fibre.

6. The Variable Aperture in the Far-Field (VAFF) Technique

6.1 Theory

The direct far-field scanning technique measures the angular distribution of the far-field intensity distribution from the single mode fibre, $|F(p)|^2$, (see section 4). The variable aperture technique also measures power in the far-field but rather than making a continuous measurement of the intensity distribution, the total power passing through a set of circular apertures is measured. It is assumed that the far-field and therefore the fibre are rotationally symmetric. The apertures are centred on the optical axis of the fibre so that they are also centred on the axis of rotational symmetry of the far-field pattern.

For a circular aperture of radius a located a distance D from the fibre endface, the half angle of the cone subtended by the aperture at the fibre endface, $\theta_{aperture}$, is given by:

$$\theta_{aperture} = \arctan\left(\frac{a}{D}\right). \qquad 6\text{-}1$$

The optical power passing through the aperture from a curved wavefront centred on the fibre endface is given by [1]:

$$P(v) = 2\pi\int_0^v F^2(p)p\,dp, \qquad 6\text{-}2$$

where $v = k\sin(\theta_{aperture})$. Since $p = k\sin(\theta)$, this equation can be re-written as:

$$P(\theta_{aperture}) \propto \int_0^{\theta_{aperture}} F^2(\theta)\sin(\theta)\cos(\theta)d\theta. \qquad 6\text{-}3$$

Equation 6-2 forms the basis for the EIA/TIA reference test method for mode-field diameter measurement by the VAFF technique [11]. However, it has been suggested that equation 6-2 is incorrect and that the appropriate version of equation 6-3 is [12]:

$$P(\theta_{aperture}) \propto \int_0^{\theta_{aperture}} F^2(\theta)\sin(\theta)d\theta, \qquad 6\text{-}4$$

where R is the distance from the fibre endface to the edge of the aperture. This is the expression that has recently appeared in ITU-T draft recommendations for an effective area test method [13]. The difference between the two expressions can be understood from Figure 13, which shows the parameters used to derive equations 6-3 and 6-4. The discrepancy arises

from which incremental length of the phase front is integrated to give the total power passing through the aperture. Equation 6-4 uses the arc length along the curved wavefront, given by $R\,\delta\theta$. However, 6-3 uses the projection of this curved section onto a plane parallel to that of the aperture, $R\,\delta\theta\cos(\theta)$. Clearly, for small angles $\cos(\theta)\approx 1$ and the difference between the two formulations is small. It has been shown that they lead to a difference in calculated MFD of typically less than 0.5% - even for dispersion shifted fibres with the smallest cores and broadest far-fields [12].

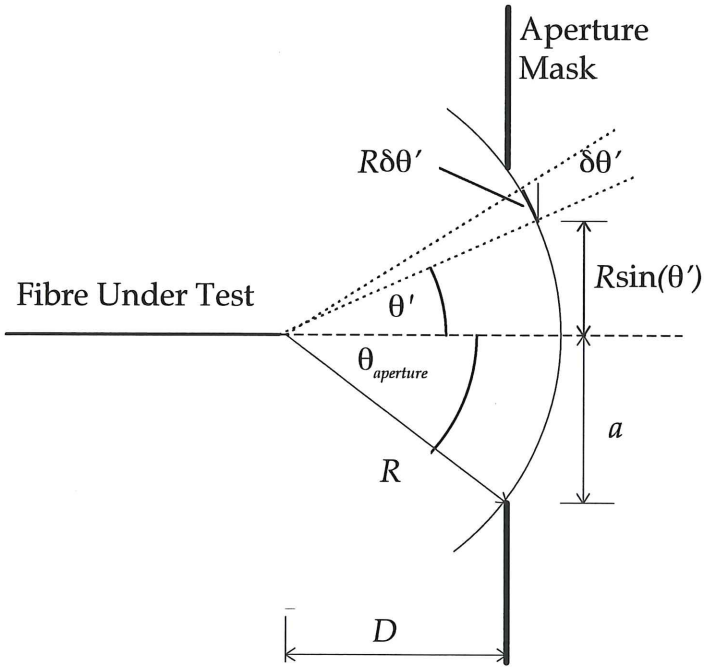


Figure 13. *Parameters used in the variable aperture in the far-field measurement technique.*

Once the aperture power function has been determined for a number of apertures, the relative far-field power distribution can be calculated from the derivative. Analysis of the data then follows the same method as that of the direct far-field method, i.e. transformation to the near-field and calculation of the effective area from the field distribution (see section 4). The far-field power distribution can be calculated using either:

$$F^2(p) \propto \frac{1}{p}\frac{dP(p)}{dp}, \qquad 6\text{-}5$$

or

$$F^2(\theta) \propto \frac{1}{\sin(\theta)}\frac{dP(\theta)}{d\theta}, \qquad 6\text{-}6$$

depending on whether the aperture power function is assumed to follow from equation 6-2 or 6-4 respectively.

6.2 Experimental Technique

The basic experimental setup for the variable aperture technique is shown below in Figure 14. Apertures of different diameters are usually precision mounted on a wheel so that they can be easily changed and the throughput power measured for each one. Figure 15 shows an example of measured VAFF data for a matched-cladding fibre.

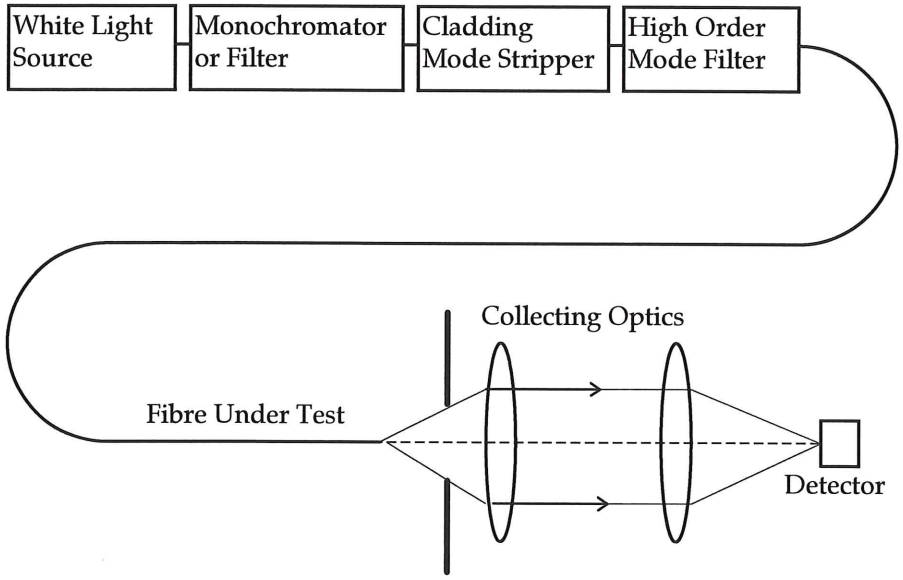


Figure 14. Basic variable aperture system (after ref. 10)

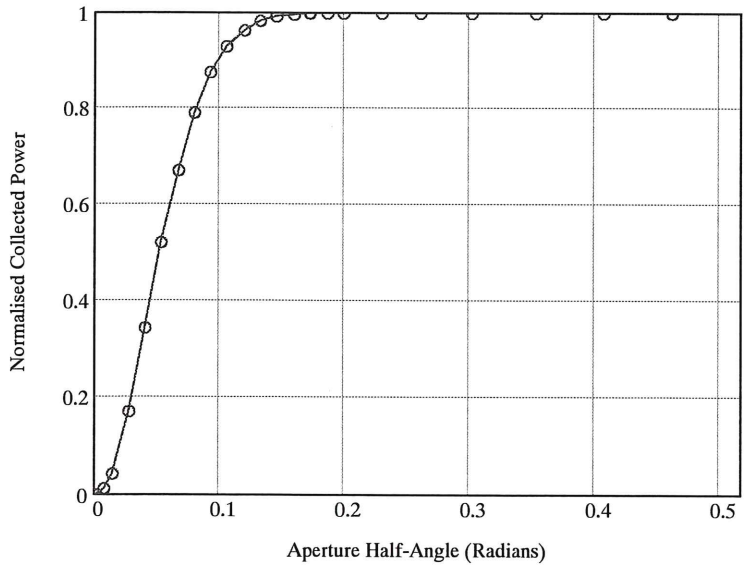


Figure 15. Example of measured variable aperture in the far-field data for a matched-cladding fibre at 1310-nm.

The equipment used in our investigations was a PK Technology S25 measurement system including an internal tungsten halogen lamp filtered using a monochromator with 10-nm spectral width. The wavelength calibration uncertainty is estimated to be less than ±2-nm. Twenty three

apertures were used, giving a range of half angles, $\theta_{aperture}$, between 0.0066 and 0.5176 radians.

6.3 Data Analysis

VAFF data was collected in the form of relative optical powers collected for each of the 23 apertures. Note that experimental data does not include a point with zero collected power for an aperture with zero diameter so this must be added manually to complete the data set. Also, for the largest apertures, noise on the experimental data can lead to fluctuations in the plateau region of the aperture power curve that imply that increasing the aperture diameter reduced the transmitted power. This equates to regions of negative far-field intensity, which is not a physical possibility. A filter was applied to all data sets to ensure that aperture power either increased or remained unchanged with increasing aperture diameter. Results are presented with and without the use of this filter.

After filtering, the initial aperture power data was curve fitted using a sliding parabolic function. This function was used to calculate the mode-field diameter by substitution into equation 6-5 to give the far-field distribution. The far-field distribution was then substituted into equation 4-4 to give the MFD. Although based on the incorrect form of the aperture power function, equation 6-5 agrees with that recommended by the TIA [10]. The MFD values calculated in this way are listed as the VAFF MFD values in the following tables.

The aperture power values were also curve-fitted using a sliding quartic function of the form:

$$P(\theta) = a\theta^4 + b\theta^3 + c\theta^2 + d\theta + e. \qquad (6\text{-}7)$$

The far-field intensity distribution was calculated from the aperture power function using equation 6-6, which is the correct aperture power relation. The far-field was then transformed to the near-field using a quadratic fitting method to interpolate between the 23 far-field points. The MFD was calculated in the far- and near-field using the same numerical routines as used with the experimental far- and near-field data. The effective area was calculated from the near-field intensity distribution using equation 2-2 and the same sliding quadratic integration routine as used for the other experimental data sets. Only one far-field intensity point was calculated from each aperture power value, i.e. only 23 far-field intensity points were calculated and used in the far-field MFD calculation. Also, no side-lobe inversion was performed before transforming to the near-field. The 23 far-field points were transformed to give 100 near-field points between zero radius and 15-μm. Only the points between zero radius and the first point with intensity less than 0.01% of the maximum value were used to calculate the near-field MFD and effective area - i.e. a 40-dB dynamic range.

The routines used were tested with data supplied by the TIA/EIA in two standards documents [10,11]. The resulting MFDs and effective areas are compared in Table 8 and Table 9. For these data sets, filtering had no effect because the aperture power values increased monotonically with aperture diameter.

	Calculated with smoothing	Calculated without smoothing	TIA Value
VAFF MFD (μm)	7.725	7.725	-
MFD from far-field (μm)	7.853	7.853	-
MFD from near-field (μm)	7.838	7.838	-
Effective Area from near-field (μm)^2	45.814	45.814	44.17

Table 8. Mode-field diameter and effective area values calculated from TIA/EIA sample data in [10]. Only the effective area is supplied with the sample data.

	Calculated with smoothing	Calculated without smoothing	TIA Value
VAFF MFD (μm)	8.155	8.155	8.163
MFD from far-field (μm)	8.154	8.154	-
MFD from near-field (μm)	8.211	8.211	-
Effective Area from near-field (μm)^2	49.953	49.953	-

Table 9. Mode-field diameter and effective area values calculated from TIA/EIA sample data in [11]. Only the mode-field diameter is supplied with the sample data.

The effective area calculated from the sample data in ref. 10 shows a discrepancy of 3.7%. However, this sample data set includes some unusual structure in the aperture power values for the smallest apertures that may have contributed to this result. The same numerical routines when tested with simulated variable aperture data generated for a noiseless Gaussian far-field gave an effective area that was accurate to within 0.7%.

Measurements were performed on all six fibres described in section 3 at two wavelengths - 1310-nm and 1550-nm. The MFDs and effective areas calculated from these measurements with and without filtering the data are given below. The Namihira factors were derived from the MFD value calculated directly from the VAFF data and the effective area calculated from the near-field.

6.3.1 Results at 1550-nm Wavelength

With Smoothing	MFD From Far-Field System (μm)	Standard Deviation (μm)	VAFF MFD (μm)	Standard Deviation (μm)	Far-Field MFD (μm)	Standard Deviation (μm)	Near-Field MFD (μm)	Standard Deviation (μm)	Effective Area (μm)^2	Standard Deviation (μm)^2	Namihira Factor, k	Standard Deviation
Attenuation Flattened	10.250	0.006	10.174	0.047	10.158	0.038	10.172	0.045	79.436	0.695	0.977	0.012
Dispersion Flattened	8.395	0.011	8.226	0.163	8.072	0.227	8.293	0.352	54.324	1.998	1.022	0.056
Matched Cladding	10.424	0.014	10.376	0.051	10.354	0.054	10.368	0.044	81.944	0.797	0.969	0.013
Dispersion Shifted	7.924	0.004	7.853	0.080	7.892	0.079	7.900	0.084	45.780	1.014	0.945	0.027
LEAF -'ve Dispersion	9.100	0.017	9.122	0.055	9.123	0.042	9.134	0.033	67.378	0.718	1.031	0.017
LEAF +'ve Dispersion	9.441	0.012	9.392	0.084	9.429	0.080	9.445	0.083	68.114	1.341	0.983	0.026
Without Smoothing												
Attenuation Flattened	10.250	0.006	10.198	0.054	10.098	0.061	10.124	0.081	79.136	0.631	0.969	0.012
Dispersion Flattened	8.395	0.011	8.413	0.214	7.804	0.301	8.216	0.315	53.296	1.567	0.959	0.054
Matched Cladding	10.424	0.014	10.394	0.054	10.300	0.067	10.322	0.037	81.774	0.569	0.964	0.012
Dispersion Shifted	7.924	0.004	7.855	0.079	7.882	0.087	7.890	0.092	45.686	1.073	0.943	0.027
LEAF -'ve Dispersion	9.100	0.017	9.141	0.052	9.091	0.052	9.101	0.042	67.017	0.838	1.021	0.018
LEAF +'ve Dispersion	9.441	0.012	9.392	0.085	9.429	0.080	9.443	0.082	68.100	1.335	0.983	0.026

Table 10. Mode-field diameters and effective areas calculated from variable aperture data at 1550-nm with and without smoothing the data to avoid negative far-field powers.

6.3.2 Results at 1310-nm Wavelength

With Smoothing	MFD From Far-Field System (μm)	Standard Deviation (μm)	VAFF MFD (μm)	Standard Deviation (μm)	Far-Field MFD (μm)	Standard Deviation (μm)	Near-Field MFD (μm)	Standard Deviation (μm)	Effective Area (μm)^2	Standard Deviation (μm)^2	Namihira Factor, k	Standard Deviation
Attenuation Flattened	9.140	0.003	9.084	0.038	9.068	0.033	9.081	0.027	63.676	0.532	0.982	0.011
Dispersion Flattened	7.016	0.012	7.031	0.019	7.049	0.016	7.059	0.018	37.718	0.233	0.971	0.008
Matched Cladding	9.257	0.016	9.199	0.031	9.169	0.065	9.167	0.077	65.410	0.341	0.984	0.008
Dispersion Shifted	6.364	0.016	6.315	0.058	6.337	0.062	6.343	0.066	29.518	0.574	0.942	0.024
LEAF -'ve Dispersion	6.678	0.045	6.665	0.015	6.682	0.029	6.678	0.030	34.157	0.311	0.979	0.010
LEAF +'ve Dispersion	7.179	0.009	7.178	0.050	7.203	0.046	7.203	0.045	38.994	0.601	0.964	0.019
Without Smoothing												
Attenuation Flattened	9.14	0.00	9.09	0.03	9.04	0.05	9.06	0.03	63.68	0.68	0.98	0.01
Dispersion Flattened	7.02	0.01	7.03	0.02	7.05	0.02	7.06	0.02	37.71	0.24	0.97	0.01
Matched Cladding	9.26	0.02	9.21	0.03	9.14	0.06	9.15	0.08	65.34	0.35	0.98	0.01
Dispersion Shifted	6.36	0.02	6.32	0.06	6.33	0.06	6.34	0.07	29.49	0.58	0.94	0.02
LEAF -'ve Dispersion	6.68	0.05	6.67	0.02	6.68	0.03	6.68	0.03	34.15	0.32	0.98	0.01
LEAF +'ve Dispersion	7.18	0.01	7.18	0.05	7.20	0.05	7.20	0.05	38.98	0.60	0.96	0.02

Table 11. Mode-field diameters and effective areas calculated from variable aperture data at 1310-nm with and without smoothing the data to avoid negative far-field powers.

6.4 Side-Lobe Inversion in Variable Aperture Data

Variable aperture consists of a limited number of aperture power values - in this case 23. When converted into far-field intensity values, these 23 points give a relatively crude representation of the angular intensity distribution compared to the far-field scan method. An example of such data is shown in Figure 16 for the attenuation-flattened fibre in the 1550-nm region. The VAFF data is compared with a far-field intensity distribution measured with the far-field scan technique. The results agree well out to the first side-lobe and then lose agreement as the variable aperture method reaches a dynamic range limit.

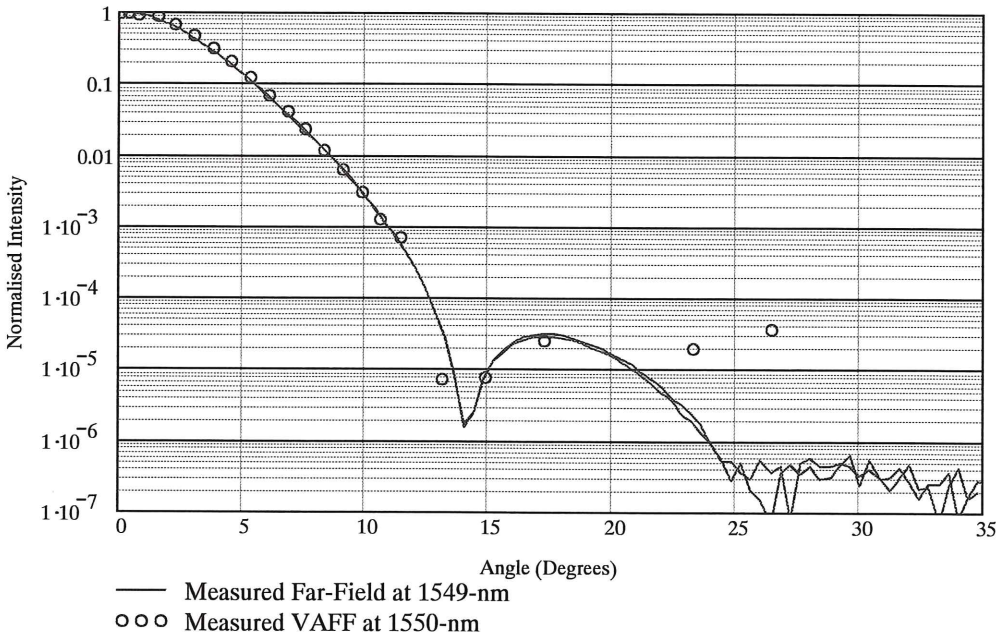


Figure 16. Far-field intensity distribution calculated from VAFF data compared with a measured far-field scan folded about zero angle. The log plot does not show two zero intensity points in the variable aperture data- one at 20.2° and the other at 29.7°.

The nature of the VAFF data makes it difficult to identify side-lobes in the far-field distribution and it is not normally practical to invert them. The far-field intensity distribution at large angles is derived from the plateau region of the VAFF aperture power data. Here small variations in aperture power due to side lobes sit on top of the high power transmitted by the largest apertures and are therefore difficult to distinguish.

Side-lobe inversion is not an issue when calculating MFD, either from the VAFF data directly or from the derived far-field using equation 2-5 since both methods use the intensity and not the amplitude of the far-field. However, it does make a significant difference to the effective area, as is evident from the values in Table 3 and Table 4. The origin of this can be appreciated from the near-field distributions shown below. Each intensity distribution is derived from a different measurement technique. The difference between Figure 17 and Figure 18 is that the side-lobes in the far-field intensity distribution were inverted before transforming to give the near-field in Figure 18.

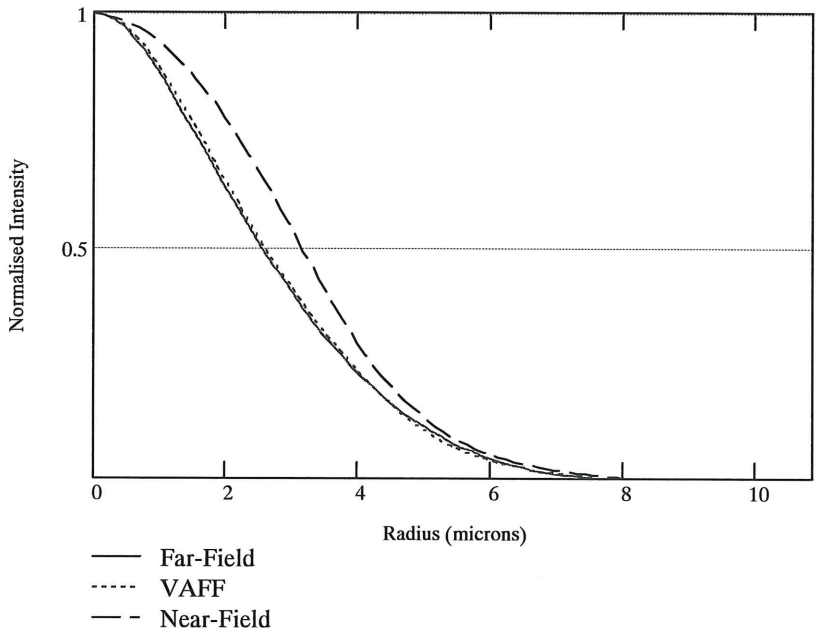


Figure 17. Near-field intensity distributions for the same attenuation-flattened fibre from three different methods. The side-lobes on the far-field data were not inverted before transforming to the near-field.

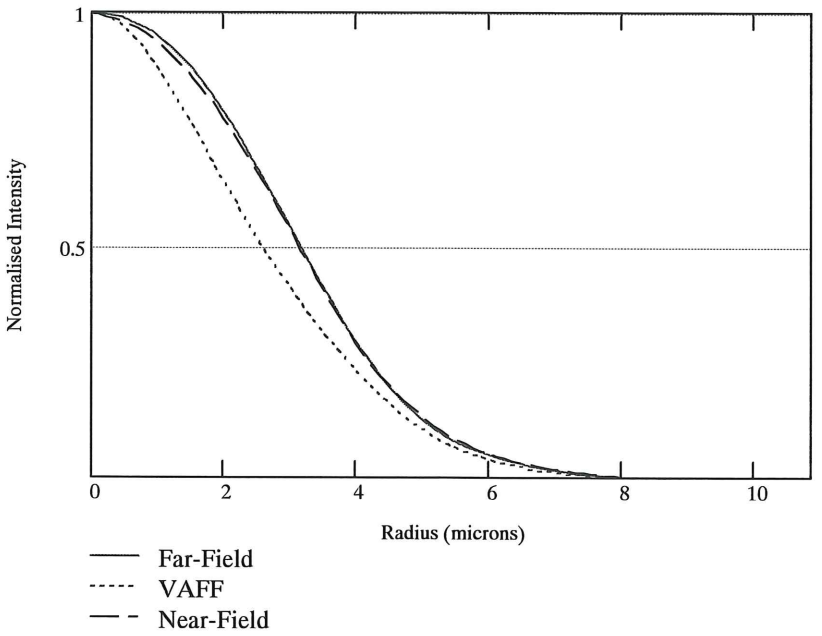


Figure 18. Near-field intensity distributions for the same attenuation-flattened fibre from three different methods. The side-lobes on the far-field data were inverted before transforming to give the near-field.

Clearly, inverting the side lobes of the far-field distribution has a significant effect on the near-field calculated from it. It is not surprising that the effective area values for inverted side lobes exceeded those for non-inverted side-lobes in Table 3 and Table 4. In comparing the effective areas calculated from far-field and VAFF measurements, the far-field values without side-lobe

inversion should be used. The difficulty in identifying and inverting side-lobes is a significant limitation on the use of the variable aperture technique for measuring effective areas of fibres that exhibit them.

7. The Transverse Offset Technique

7.1 Theory

When two single mode fibres are butted together to form a joint, the fundamental mode field of the source fibre is coupled into the modes of the recipient fibre. These recipient modes consist of the fundamental mode, lossy cladding modes and radiation modes. The magnitude of the source mode field coupled into each recipient mode is given by the overlap integral of the two modal electric fields. In the transverse offset technique, we are concerned with the transfer of optical power from the source mode into the same mode of an identical fibre when their axes are parallel but laterally offset from each other.

The power coupled from the fundamental mode of the source fibre into the same mode of an identical recipient fibre is given by the square of the field overlap integral, $C(u)$. With reference to Figure 19,the overlap integral can be expressed as [1]:

$$C(u) = \iint_S E_a(|\mathbf{r}|)E_a(|\mathbf{r} - \mathbf{u}|)d\mathbf{r} \qquad 7\text{-}1$$

where $u = |\mathbf{u}|$ is the magnitude of the separation of the fibre axes. The integral should be performed over the region S, which extends over all space.

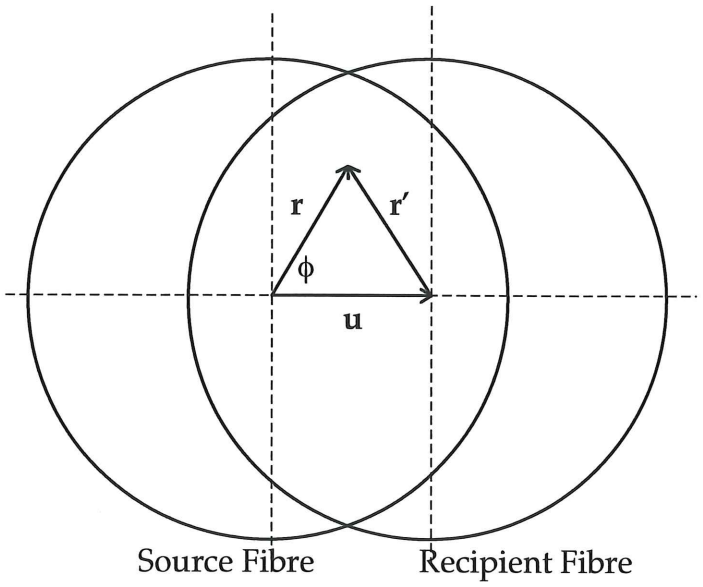


Figure 19. Geometry of the overlap integral in the transverse offset technique.

The overlap integral can be expressed as a convolution in polar co-ordinates , such that:

$$C(u) = \int_0^{2\pi}\int_0^{\infty} E_a(r)E_a(r')r\,dr\,d\phi = \left[E_a(r) * E_a(r)\right]_{r=u} \qquad 7\text{-}2$$

where $r'^2 = u^2 + r^2 - 2ru\cos(\phi)$, $r' = |\mathbf{r}'|$, $r = |\mathbf{r}|$ and the $*$ represents a 2-dimensional convolution. The Hankel transform of the convolution is [14]:

$$\mathrm{H}\{C(u)\} = \mathrm{H}\{E_a(r) * E_a(r)\} = F^2(p) \qquad 7\text{-}3$$

where $F^2(p)$ is the far-field power distribution of the fibre. Through equation 7-3, the measured power transfer function for the offset splice, $C^2(u)$, can be related to the near-field of the fundamental mode via the far-field power distribution. The near-field distribution can then be used to calculate the effective area, as described in section 2. The mode-field diameter of the fibre can be calculated directly from the power transmission function using [14]:

$$MFD_{TO} = 2\sqrt{-\frac{C^2(0)}{\frac{d^2(C^2(0))}{du^2}}} \qquad 7\text{-}4$$

7.2 Experimental Technique

The transverse offset system constructed at NPL is shown in Figure 20. A sample of test fibre was cleaved and checked with an interferometer to ensure that the cleaved endfaces were perpendicular to the fibre axis to within 0.5°. The fibre samples were then mounted in vacuum chucks facing each other and actively aligned using an xyz flexure stage to maximise the detected signal. The endfaces were brought as close together as possible without making contact. The separation was typically less than 5-μm. The lateral offset between the fibre axes was then scanned using the piezo actuator attached to one of the vacuum chucks.

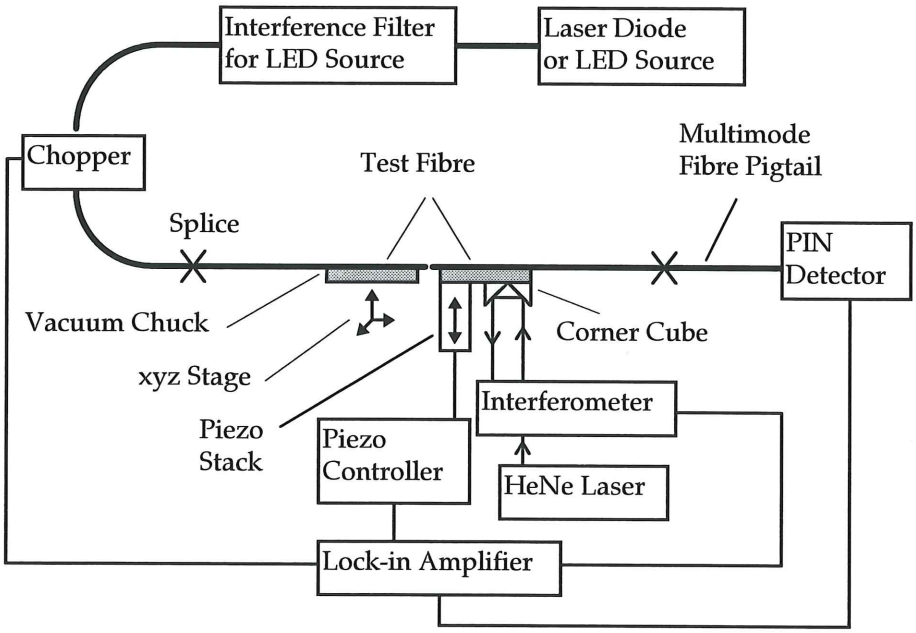


Figure 20. *Transverse offset system used at NPL to record the power transferred between two cleaved samples of fibre.*

The position of the scanning fibre was monitored by measuring the output from an interferometer. Scanning was automated by using the lock-in amplifier to drive the piezo controller and read the output signals from the interferometer and the throughput power detector. The range of travel of the piezo stack was limited to approximately 15-μm - meaning that at least two scans were required to cover enough range to measure a complete transmission curve. The constituent scans were fitted together manually to generate a complete power transmission curve. An example of a power transmission curve starting from a point just to one side of the peak transmission is shown in Figure 21.

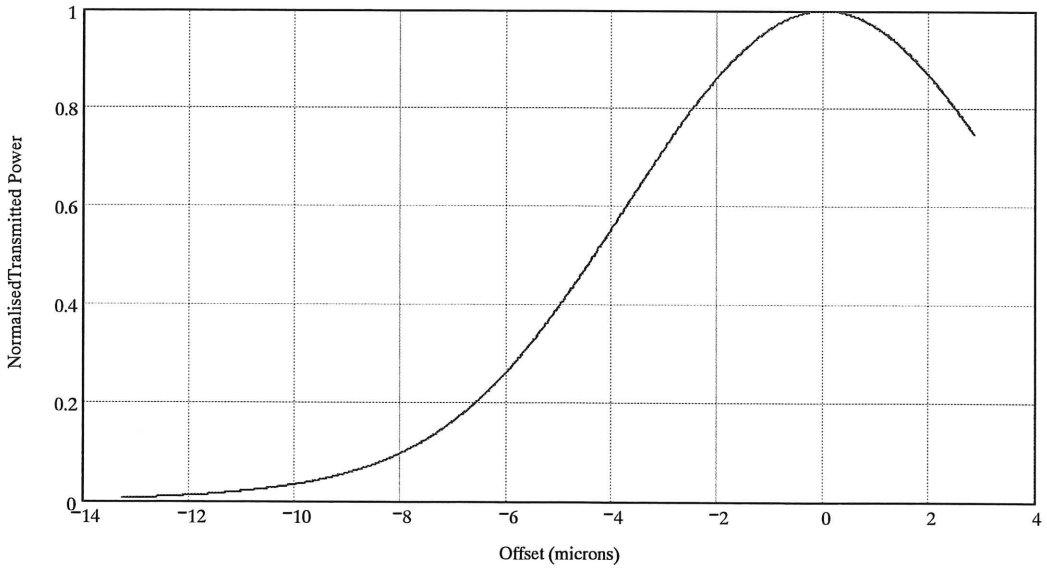


Figure 21. *Example of measured transverse offset power transmission curve for the dispersion-flattened fibre.*

7.3 Data Analysis

No reference data was found for this technique in the literature, so the numerical routines could not be checked against standards documents as for the previous three techniques. The routines were therefore checked for consistency using simulated data. A Gaussian power transmission function was generated to simulate $C^2(u)$. The scan width was set to a range of values to define optical dynamic ranges of between 20-dB and 100-dB. In all cases, the MFD of the simulated fibre was calculated using equation 7-4 to be 9.051-μm, which gives an effective area of 64.34-(μm)^2. The MFD was calculated firstly using equation 7-4 with the simulated scan data by fitting a polynomial to the transmission function of the form:

$$C^2(u) = \sum_{n=0}^{4} a_n u^{2n} \qquad 7\text{-}5$$

The MFD value calculated from the fitted curve was dependent on the width of the peak region to which the curve was fitted. On noiseless simulated Gaussian data, the error in the MFD decreased as the curve was fitted to smaller regions around the peak, as illustrated in Figure 22.

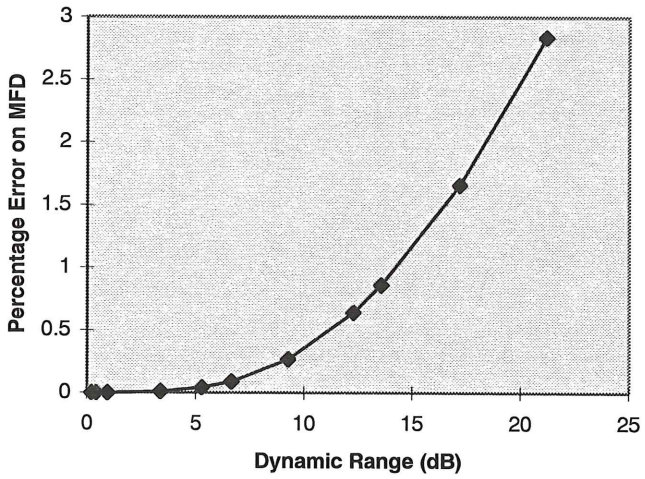


Figure 22. Percentage error on the MFD calculated from a simulated Gaussian transverse offset transmission function. The error is plotted as a function of the dynamic range of the data used to fit a polynomial to the peak.

Experimental data included noise, which tended to reduce the accuracy of the fitted curve when a very limited data point range was used. Consequently, 3-dB was chosen as the dynamic range for curve fitting such that the polynomial was fitted to the data points to either side of the peak at which the transmitted power exceeded half of the value for zero lateral offset between the fibres.

The simulated Gaussian scan data was transformed to give the far-field power distribution using equation 7-3 the MFD calculated from $F^2(p)$ using

equation 2-5. The far-field was then transformed to the near-field and the MFD and effective area calculated from equations 2-4 and 2-2 respectively. The resulting MFD values in each case were compared with the exact values and the errors are shown in Figure 23 and Figure 24.

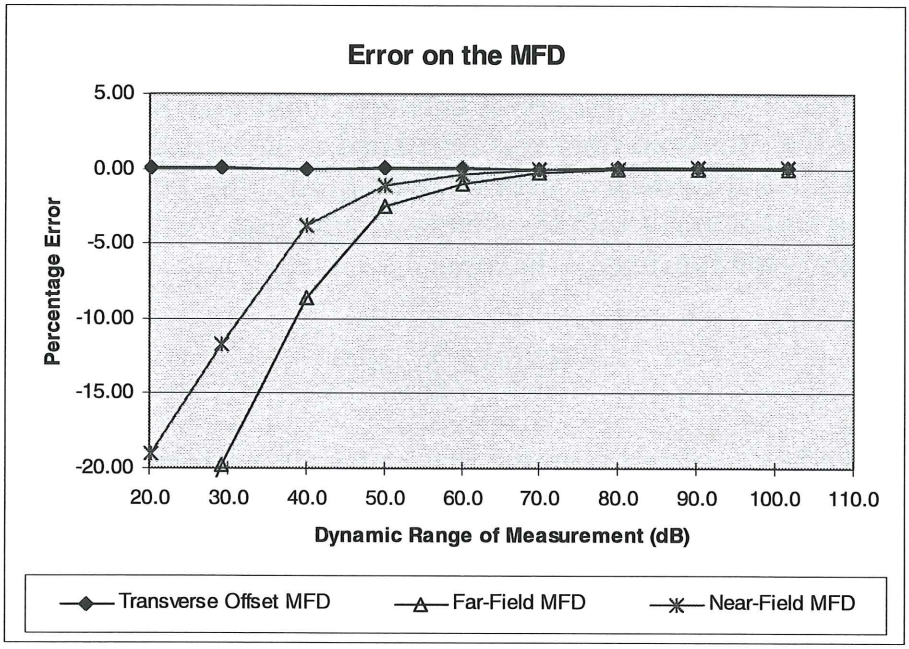


Figure 23. *Percentage errors on mode field diameters calculated from simulated transverse offset data versus dynamic range of the measured optical power.*

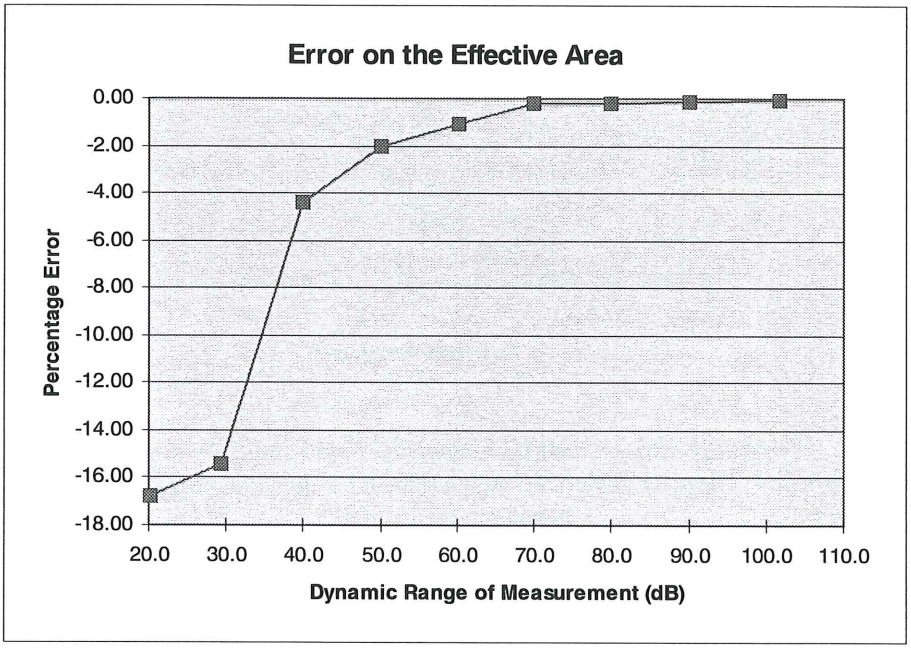


Figure 24. *Percentage errors on effective area calculated from simulated transverse offset data versus dynamic range of the measured optical power.*

It can be seen from these results that a dynamic range in excess of 70-dB is necessary to reduce errors to less than 1%. The main cause of this strict requirement is that the measured power corresponds to $C^2(u)$ and therefore

the dynamic range is immediately halved by taking the square root before transforming to the far-field. The requirement of 70-dB dynamic range for the simulated Gaussian transverse offset transmission function used here equates to a scan range of approximately ±18-μm from the peak of the function. Such a scan range was achieved for the dispersion flattened fibre by combining two overlapping scans of 15-μm width performed at 1549-nm. The resulting power transmission function is shown in Figure 25.

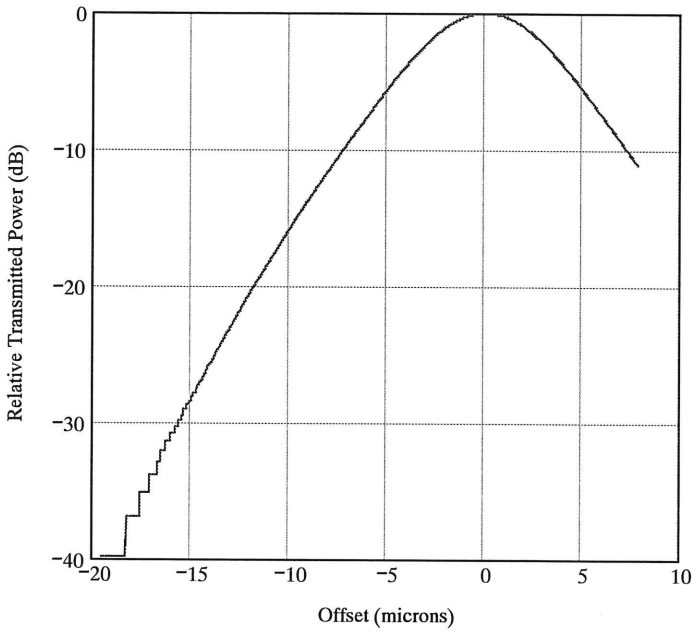


Figure 25. *Measured transverse offset power transmission data constructed from two overlapping 15-μm scans.*

The MFD calculated directly from the polynomial fitted to this transmission curve was 8.09-μm, compared to 8.40-μm from the far-field scan method. When transformed to the far-field using equation 7-3, the MFD was 7.61-μm. Transforming from the far-field to the near-field gave an MFD of 7.87-μm and effective area of 46.51-μm^2 compared with 53.84-μm^2 from the far-field scan method. The suppressed values of MFD and A_{eff} in the far- and near-fields are consistent with the lack of sufficient dynamic range as demonstrated in Figure 23 and Figure 24 for the simulated Gaussian data.

The transverse offset technique was found to be highly sensitive to vibration of the optical system - making it difficult to perform in practice. The MFD calculated from the power transmission curve was also highly dependent on the separation of the fibre endfaces, as illustrated in Figure 26 for the dispersion-flattened fibre. The two fibre endfaces were initially butted together and then pulled apart by distances measured using a linear variable differential transformer.

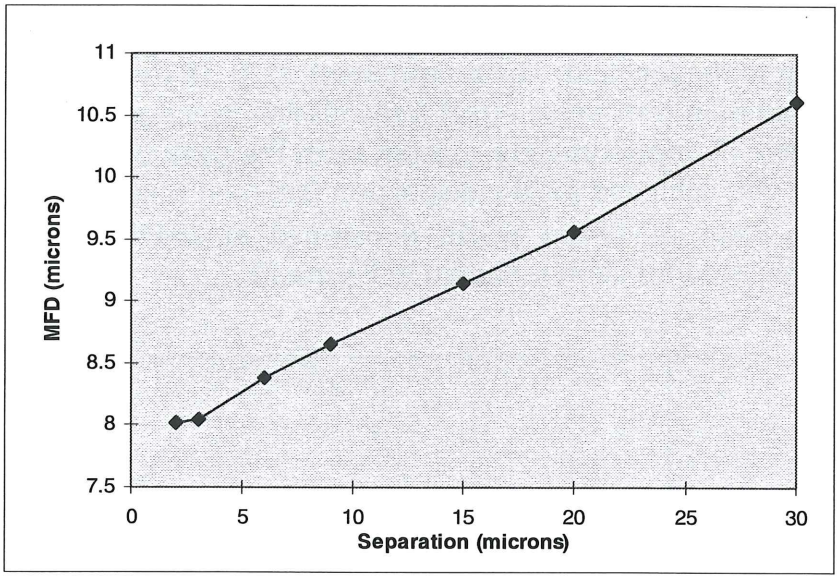


Figure 26. *MFD measured by the transverse offset method versus fibre endface separation.*

8. Summary of results

The mode field diameters, effective areas and Namihira factors calculated from the three most successful measurement techniques are summarised below. The far-field values quoted are for inverted side-lobes, where present, and the variable aperture values are those with smoothing of the large aperture data.

8.1 1549/1550-nm Results

MFD

Fibre	1549-nm		1549-nm		1550-nm	
	Far-Field	Std. Dev.	Near-Field	Std. Dev.	VAFF	Std. Dev.
Attenuation Flattened	10.249	0.015	10.384	0.075	10.174	0.047
Dispersion Flattened	8.394	0.016	-	-	8.226	0.163
Matched Cladding	10.423	0.019	10.483	0.038	10.376	0.051
Dispersion Shifted	7.923	0.008	7.997	0.076	7.853	0.080
LEAF -'ve Dispersion	9.099	0.023	9.218	0.081	9.122	0.055
LEAF +'ve Dispersion	9.440	0.052	9.607	0.130	9.392	0.084

Effective Area

Fibre	1549-nm		1549-nm		1550-nm	
	Far-Field	Std. Dev.	Near-Field	Std. Dev.	VAFF	Std. Dev.
Attenuation Flattened	80.936	0.227	80.630	0.226	79.436	0.695
Dispersion Flattened	53.835	0.197	-	-	54.324	1.998
Matched Cladding	83.391	0.305	83.042	0.307	81.944	0.797
Dispersion Shifted	46.050	0.089	45.715	0.089	45.780	1.014
LEAF -'ve Dispersion	67.250	0.295	66.733	0.305	67.378	0.718
LEAF +'ve Dispersion	68.399	0.580	67.888	0.574	68.114	1.341

Namihira Factor

Fibre	1549-nm		1549-nm		1550-nm	
	Far-Field	Std. Dev.	Near-Field	Std. Dev.	VAFF	Std. Dev.
Attenuation Flattened	0.981	0.003	0.973	0.017	0.977	0.012
Dispersion Flattened	0.973	0.004	-	-	1.022	0.056
Matched Cladding	0.977	0.004	0.973	0.009	0.969	0.013
Dispersion Shifted	0.934	0.002	0.928	0.023	0.945	0.027
LEAF -'ve Dispersion	1.034	0.006	1.026	0.029	1.031	0.017
LEAF +'ve Dispersion	0.977	0.008	0.968	0.037	0.983	0.026

Table 12. Summary of MFD, A_{eff} and k_{Nam} values calculated near 1550-nm.

Fibre Numbers:

1 Lucent All Wave
2 Lucent True Wave
3 Corning Matched Cladding
4 Sumitomo Dispersion Shifted
5 Corning Submarine LEAF -'ve Dispersion
6 Corning Terrestrial LEAF +'ve Dispersion

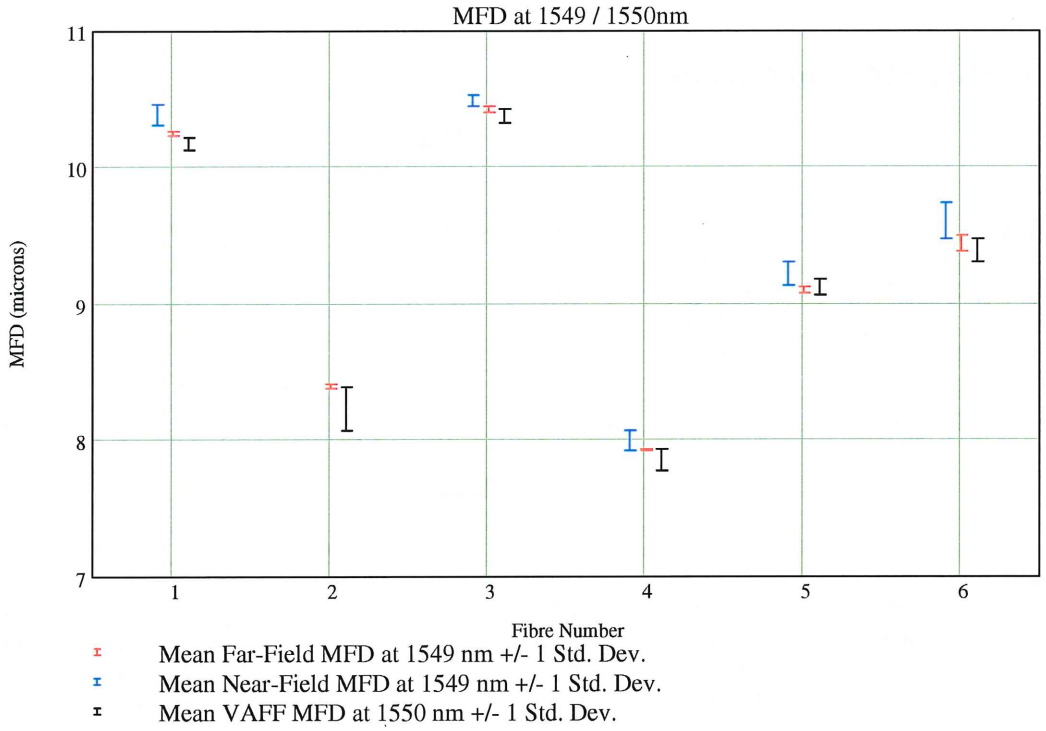


Figure 27. Mode field diameter values measured for six different fibres near 1550-nm by three different methods. Error bars represent ± one standard deviation from the mean.

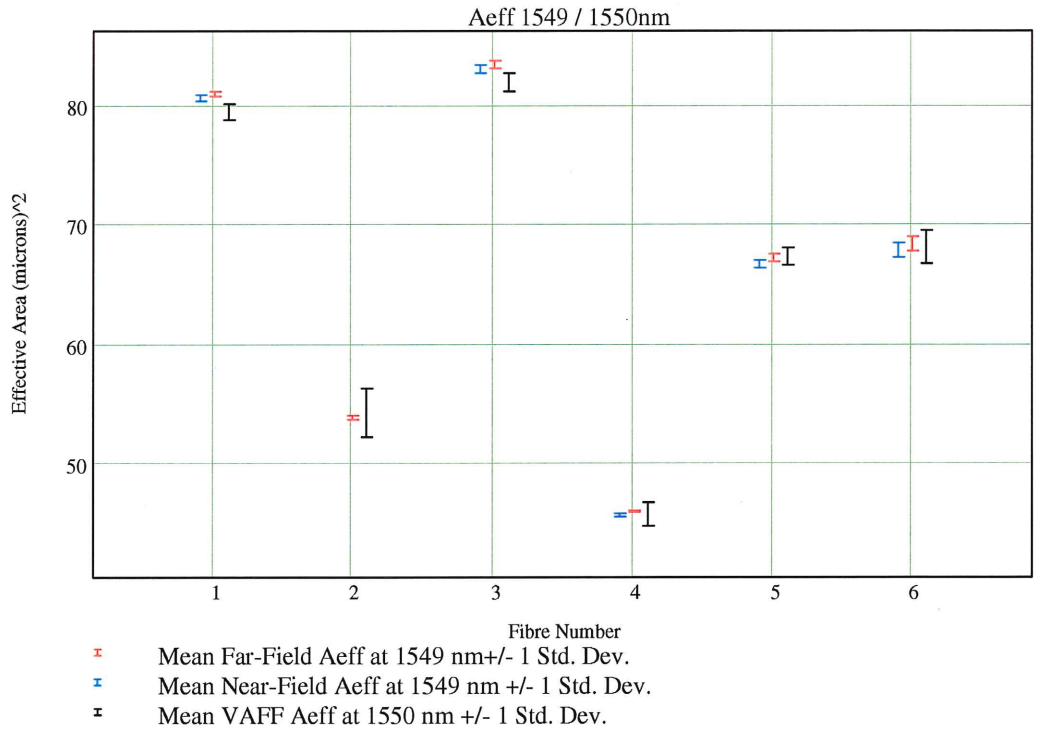


Figure 28. Effective area values measured for six different fibres near 1550-nm by three different methods. Error bars represent ± one standard deviation from the mean.

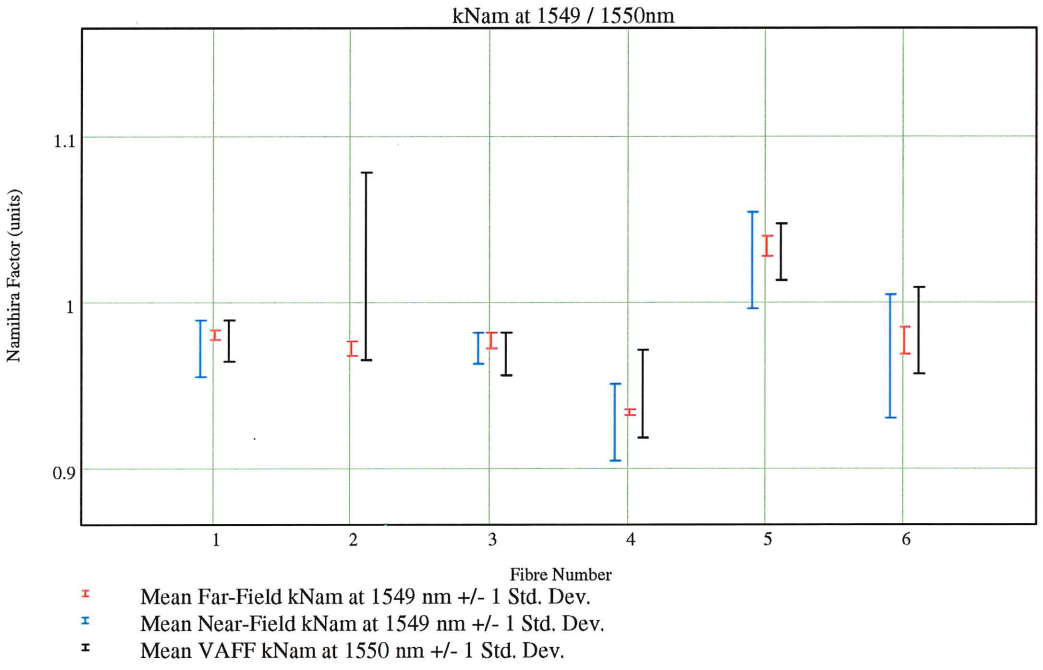


Figure 29. Namihira factors measured for six different fibres near 1550-nm by three different methods. Error bars represent ± one standard deviation from the mean.

8.2 1309.2/1310-nm Results

MFD

Fibre	1309-nm Far-Field	Std. Dev.	1309-nm Near-Field	Std. Dev.	1310-nm VAFF	Std. Dev.
Attenuation Flattened	9.138	0.009	9.223	0.075	9.084	0.038
Dispersion Flattened	7.015	0.015	7.078	0.043	7.031	0.019
Matched Cladding	9.256	0.018	9.385	0.112	9.199	0.031
Dispersion Shifted	6.363	0.017	6.415	0.048	6.315	0.058
LEAF -'ve Dispersion	6.677	0.053	6.744	0.060	6.665	0.015
LEAF +'ve Dispersion	7.178	0.027	7.266	0.085	7.178	0.050

Effective Area

Fibre	1309-nm Far-Field	Std. Dev.	1309-nm Near-Field	Std. Dev.	1310-nm VAFF	Std. Dev.
Attenuation Flattened	66.385	0.132	66.182	0.131	63.676	0.532
Dispersion Flattened	38.467	0.141	38.257	0.147	37.718	0.233
Matched Cladding	67.786	0.267	67.569	0.267	65.410	0.341
Dispersion Shifted	29.747	0.157	29.562	0.164	29.518	0.574
LEAF -'ve Dispersion	34.107	0.538	33.875	0.530	34.157	0.311
LEAF +'ve Dispersion	38.841	0.260	38.567	0.258	38.994	0.601

Namihira Factor

Fibre	1309-nm Far-Field	Std. Dev.	1309-nm Near-Field	Std. Dev.	1310-nm VAFF	Std. Dev.
Attenuation Flattened	1.012	0.002	1.004	0.020	0.982	0.011
Dispersion Flattened	0.995	0.005	0.987	0.015	0.971	0.008
Matched Cladding	1.007	0.005	0.998	0.031	0.984	0.008
Dispersion Shifted	0.935	0.006	0.929	0.018	0.942	0.024
LEAF -'ve Dispersion	0.974	0.020	0.964	0.025	0.979	0.010
LEAF +'ve Dispersion	0.960	0.007	0.950	0.030	0.964	0.019

Table 13. Summary of MFD, A_{eff} and k_{Nam} values calculated near 1310-nm.

Fibre Numbers:

1 Lucent All Wave
2 Lucent True Wave
3 Corning Matched Cladding
4 Sumitomo Dispersion Shifted
5 Corning Submarine LEAF -'ve Dispersion
6 Corning Terrestrial LEAF +'ve Dispersion

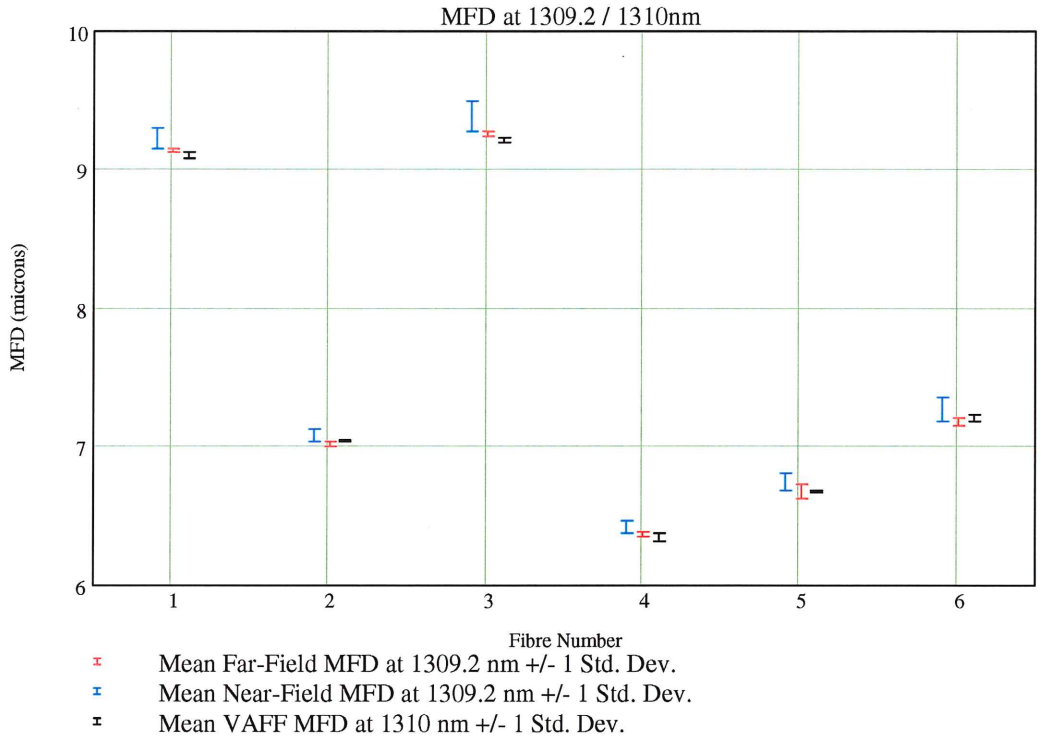


Figure 30. Mode field diameter values measured for six different fibres near 1310-nm by three different methods. Error bars represent ± one standard deviation from the mean.

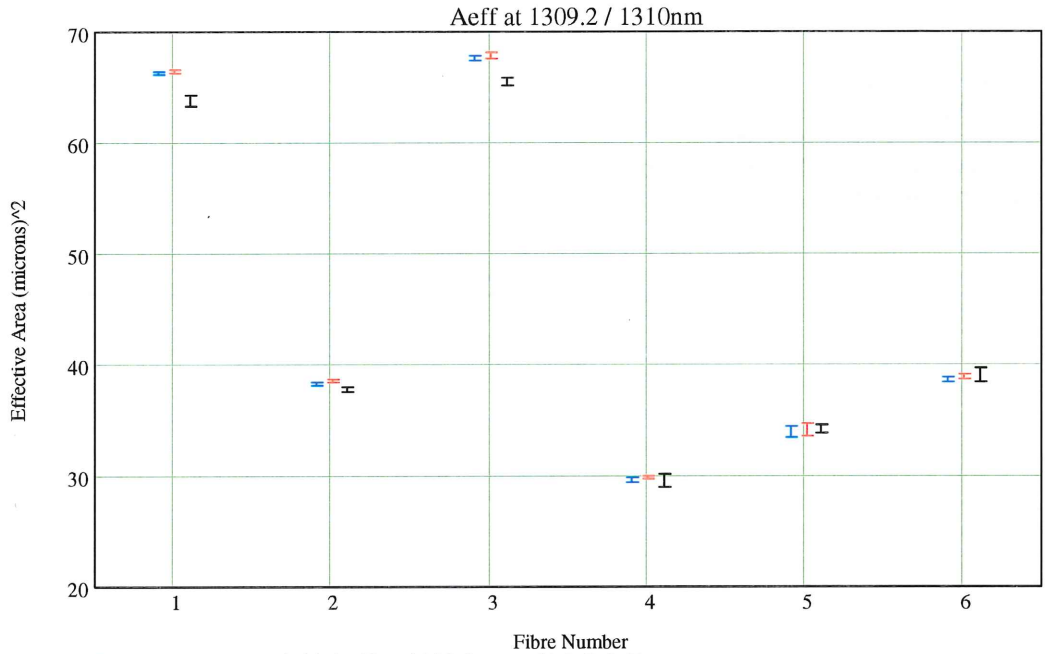


Figure 31. Effective area values measured for six different fibres near 1310-nm by three different methods. Error bars represent ± one standard deviation from the mean.

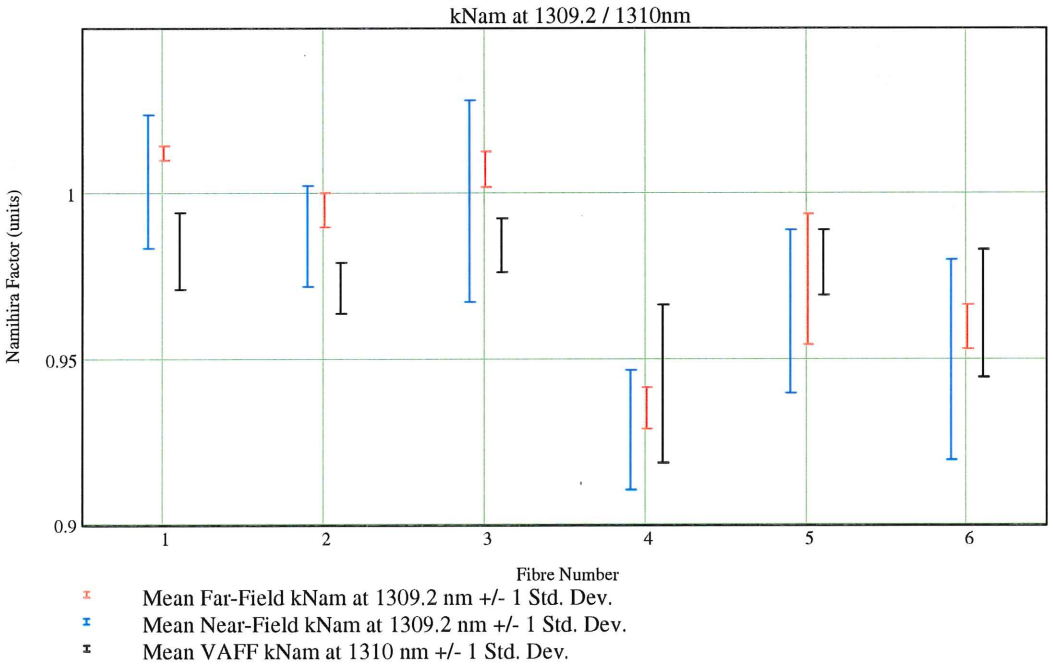


Figure 32. Namihira factors measured for six different fibres near 1310-nm by three different methods. Error bars represent ± one standard deviation from the mean.

9. Conclusions

Four different methods were used to measure the mode-field diameters and effective areas of single mode fibres in the 1550-nm and 1310-nm regions. Of the four techniques, the far-field scan was generally found to give the best repeatability. The equipment used to perform the far-field measurements exists as an established MFD system at NPL and has therefore been chosen as the basis for the effective area measurement service.

The far-field data was processed with and without inversion of the side-lobes in the distribution. For the attenuation-flattened, dispersion-flattened and matched-cladding fibres, side-lobe inversion made a significant difference to the effective area. Inverting the side-lobes increased the measured effective area of these fibres by 2-3% at 1549-nm and 3-4% at 1309.2-nm. These increases are reflected in the Namihira factors calculated using the effective area and the MFD in the far-field, which is unaffected by side-lobe inversion. Namihira makes no reference to inverting the side-lobes when calculating effective areas from VAFF data. This is expected to lead to an underestimate of the effective area and therefore of the correction factor.

The far-field method gives sufficient detail to allow inversion of side-lobes if required. It was demonstrated in Figure 17 and Figure 18 that near-fields calculated from far-field data can be made to agree with those from either VAFF or direct near-field measurements. The far-field method is therefore the most flexible option with regard to comparisons between different techniques for measuring effective area.

There exist a number of issues regarding numerical methods in processing the experimental data from all of these methods. In particular, the Hankel transform plays a pivotal role in all but the near-field method. The transverse offset technique is particularly sensitive to errors in the evaluation of the transform and served to illustrate the requirement for high dynamic range in measured data to be transformed. A fast analytic implementation of the transform can be achieved if the data can be sufficiently approximated by a set of uniform steps. This is possible for far-field and transverse offset measurements but not for VAFF, where the data points are relatively sparse and must be interpolated. The transform itself is not a one-to-one mapping between domains such as the far- and near-fields. A near-field of arbitrary extent can be calculated from any far-field distribution. Care must be taken in choosing a range of destination co-ordinates, such as near-field radii that are appropriate to the dynamic range of the far-field distribution available. This is particularly important when the MFD or effective area are to be calculated from the resulting near-field.

There is a great deal of scope for further investigating the numerical methods appropriate to effective area measurement. In particular, the development of fast and robust Hankel transform routines and the choice of appropriate limits for the effective area integral based on the dynamic range of the measured

data. These issues will be pursued in more detail within the context of the development of the effective area measurement service based on the far-field scan technique.

10. References

1 Artiglia M. *et al.*, "Mode Field Diameter Measurements in Single-Mode Optical Fibres", IEEE Journal of Lightwave Technology, **7**, *pp.* 1139-1152, (1989).

2 ITU COM 15-273-E "Definition and Test Methods for the Relevant Parameters of Sngle-Mode Fibres - Appendix on Nonlinearities for G.650", (1996).

3 Namihira Y., "Relationship Between Nonlinear Effective Area and Modefield Diameter for Dispersion Shifted Fibres", Electronics Letters, **30**, *pp.* 262-263, (1994).

4 Namihira Y., "Comparison of Wavelength Dependence of Correction of Effective Area and MFD for Large Effective Area Fibers with Dispersion Shifted Fibers", Proceedings of the 4th Optical Fibre Measurement Conference, NPL, Teddington, *pp.* 187-190, (1997).

5 Namihira Y., "Measurement Results of Effective Area (Aeff) and MFD and their Correction Factor for Non-Zero Dispersion Shifted Fibres (NZFs, G.655) and Dispersion Shifted Fibres (DSFs, G.653) by Using Variable Aperture Technique", ITU Com 15-53-E, (1997).

6 Namihira Y., "Wavelength Dependence of Correction Factor on Effective Area and Mode Field Diameter for Various Singlemode Optical Fibres", Electronics Letters, **33**, *pp.* 1483-1485, (1997).

7 Wittman R. C. and Young M., "Are the Formulas for Mode-Field Correct?", Technical Digest of the Symposium on Optical Fibre Measurements, Boulder, Colorado, *pp.* 141-144, (1998).

8 Anonymous, "EIA/TIA FOTP-164 Single-Mode Fiber, Measurement of Mode Field Diameter by Far-Field Scanning", (1991).

9 ITU-T COM 15-R 68-E, "Draft Revised ITU-T Recommendation G.650 - Definition and Test Methods for the Relevant Parameters of Single-Mode Fibres", (1996).

10 Anonymous, "EIA/TIA FOTP-132 Measurement of the Effective Area of Single-Mode Optical Fiber", (1998).

11 Anonymous, "EIA/TIA FOTP-167 Mode Field Diameter, Variable Aperture in the Far Field", (1992).